

# New Results from the Studies of the $N(1440)1/2^+$ , $N(1520)3/2^-$ , and $\Delta(1620)1/2^-$ Resonances in Exclusive $ep \rightarrow e'p'\pi^+\pi^-$ Electroproduction with the CLAS Detector

V.I. Mokeev,<sup>1,2,\*</sup> V.D. Burkert,<sup>1</sup> D.S. Carman,<sup>1</sup> L. Elouadrhiri,<sup>1</sup> G.V. Fedotov,<sup>3,2</sup>  
E.N. Golovatch,<sup>2</sup> R.W. Gothe,<sup>3</sup> K. Hicks,<sup>4</sup> B.S. Ishkhanov,<sup>2</sup> E.L. Isupov,<sup>2</sup> and Iu. Skorodumina<sup>3,2</sup>

<sup>1</sup>Thomas Jefferson National Accelerator Facility, Newport News, Virginia 23606

<sup>2</sup>Skobeltsyn Nuclear Physics Institute and Physics Department at Moscow State University, 119899 Moscow, Russia

<sup>3</sup>University of South Carolina, Columbia, South Carolina 29208

<sup>4</sup>Ohio University, Athens, Ohio 45701

(Dated: June 27, 2018)

The transition helicity amplitudes from the proton ground state to the  $N(1440)1/2^+$ ,  $N(1520)3/2^-$ , and  $\Delta(1620)1/2^-$  resonances ( $\gamma_v p N^*$  electrocouplings) were determined from the analysis of nine independent one-fold differential  $\pi^+\pi^-p$  electroproduction cross sections off a proton target, taken with CLAS at photon virtualities  $0.5 \text{ GeV}^2 < Q^2 < 1.5 \text{ GeV}^2$ . The phenomenological reaction model employed for separation of the resonant and non-resonant contributions to this exclusive channel was further developed. The  $N(1440)1/2^+$ ,  $N(1520)3/2^-$ , and  $\Delta(1620)1/2^-$  electrocouplings were obtained from the resonant amplitudes of charged double-pion electroproduction off the proton in the aforementioned area of photon virtualities for the first time. Consistent results on  $\gamma_v p N^*$  electrocouplings available from independent analyses of several  $W$ -intervals with different non-resonant contributions offer clear evidence for the reliable extraction of these fundamental quantities. These studies also improved the knowledge on hadronic branching ratios for the  $N(1440)1/2^+$ ,  $N(1520)3/2^-$ , and  $\Delta(1620)1/2^-$  decays to the  $\pi\Delta$  and  $\rho N$  final states. These new results provide a substantial impact on the QCD-based approaches that describe the  $N^*$  structure and demonstrate the capability to explore fundamental ingredients of the non-perturbative strong interaction that are behind the excited nucleon state formation.

PACS numbers: 11.55.Fv, 13.40.Gp, 13.60.Le, 14.20.Gk

## I. INTRODUCTION

The studies of transition amplitudes from the ground to excited nucleon states off the proton ( $\gamma_v p N^*$  electrocouplings) offer insight into the  $N^*$  structure and allow the exploration of the non-perturbative strong interaction mechanisms that are responsible for the resonance formation as relativistic bound systems of quarks and gluons [1–3]. The data on  $\gamma_v p N^*$  electrocouplings represent the only source of information on different manifestations of the non-perturbative strong interaction in the generation of excited nucleon states of different quantum numbers.

The CLAS detector at Jefferson Lab is a unique large-acceptance instrument designed for the comprehensive exploration of exclusive meson electroproduction. It offers excellent opportunities for the study of electroexcitation of nucleon resonances in detail and with precision. The CLAS detector has provided the dominant portion of all data on meson electroproduction in the resonance excitation region. The studies of transition helicity amplitudes from the proton ground state to its excited states represent a key aspect of the  $N^*$  program with CLAS [1, 4–6].

Meson-electroproduction data off nucleons in the  $N^*$

region obtained with CLAS open up an opportunity to determine the  $Q^2$ -evolution of the  $\gamma_v N N^*$  electrocouplings in a combined analysis of various meson-electroproduction channels for the first time. A variety of measurements of  $\pi^+n$  and  $\pi^0p$  single-pion electroproduction off the proton, including polarization measurements, have been performed with CLAS in the range of  $Q^2$  from 0.16 to 6  $\text{GeV}^2$  and in the area of invariant masses of the final hadrons  $W < 2.0 \text{ GeV}$  [7–15]. Exclusive  $\eta p$  electroproduction off the proton was studied with CLAS for  $W < 2.3 \text{ GeV}$  and  $Q^2$  from 0.2 to 3.1  $\text{GeV}^2$  [16]. Furthermore, differential cross section and polarization asymmetries in exclusive  $KY$  electroproduction channels were obtained for  $W$  from threshold to 2.6  $\text{GeV}$  and for  $Q^2 < 5.4 \text{ GeV}^2$  [17–22]. These experiments were complemented by the measurements of nine independent  $\pi^+\pi^-p$  electroproduction cross sections off the proton. The data on charged double-pion electroproduction covered the area of  $W < 1.6 \text{ GeV}$  at photon virtualities from 0.25 to 0.55  $\text{GeV}^2$  [23]. They are also available from earlier measurements with CLAS for  $W$  from 1.40  $\text{GeV}$  to 2.10  $\text{GeV}$  and  $0.5 \text{ GeV}^2 < Q^2 < 1.5 \text{ GeV}^2$  [24].

The electroexcitation amplitudes for the low-lying resonances  $\Delta(1232)3/2^+$ ,  $N(1440)1/2^+$ ,  $N(1520)3/2^-$ , and  $N(1535)1/2^-$  were determined over a wide range of  $Q^2$  in a comprehensive analysis of JLab-CLAS data on differential cross sections, longitudinally polarized beam asymmetries, and longitudinal target and beam-target asymmetries [25]. Recently  $\gamma_v N N^*$  electrocouplings of several higher-lying nucleon resonances:  $N(1675)5/2^-$ ,

\*Current address: Thomas Jefferson National Accelerator Facility, Newport News, Virginia 23606

$N(1680)5/2^+$ , and  $N(1710)1/2^+$  have become available for the first time for  $1.5 \text{ GeV}^2 < Q^2 < 4.5 \text{ GeV}^2$  from analysis of exclusive  $\pi^+n$  electroproduction off the proton [15]. Electrocouplings for the  $N(1440)1/2^+$  and  $N(1520)3/2^-$  resonances for  $Q^2 < 0.6 \text{ GeV}^2$  have been determined from the data on exclusive  $\pi^+\pi^-p$  electroproduction off the proton [27] together with the preliminary results on the electrocouplings of several resonances in the mass range from 1.6 GeV to 1.75 GeV available for the first time from this exclusive channel at  $0.5 \text{ GeV}^2 < Q^2 < 1.5 \text{ GeV}^2$  [2, 5]. The CLAS results on the  $\gamma_v p N^*$  electrocouplings [1, 5, 15, 25, 27] have had a stimulating impact on the theory of the excited nucleon state structure, in particular, on the QCD-based approaches.

The light cone sum rule (LCSR) approach [28, 29] for the first time provided access to the quark distribution amplitudes (DA) inside the  $N(1535)1/2^-$  resonance from analysis of the CLAS results on the  $\gamma_v p N^*$  electrocouplings of this state [25]. Confronting the quark DA's of excited nucleon states determined from the experimental results on the  $\gamma_v p N^*$  electrocouplings to the LQCD expectations, makes it possible to explore the emergence of the resonance structure starting from the QCD Lagrangian. The moments of the  $N(1535)1/2^-$  quark DA's derived from the CLAS data are consistent with the LQCD expectations [30].

The Dyson-Schwinger Equations of QCD (DSEQCD) provide a conceptually different avenue for relating the  $\gamma_v p N^*$  electrocouplings to the fundamental QCD Lagrangian [31–34]. The DSEQCD approach allows for the evaluation of the contribution of the three bound dressed quarks, the so-called quark core, to the structure of excited nucleon states starting from the QCD Lagrangian. A successful description of the nucleon elastic form factors and the CLAS results on the  $N \rightarrow \Delta$ ,  $N \rightarrow N(1440)1/2^+$  transition electromagnetic form factors [1, 5, 25, 27] at photon virtualities  $Q^2 > 2.0 \text{ GeV}^2$  has been recently achieved within the DSEQCD framework [31, 33, 35]. However, at smaller photon virtualities  $Q^2 < 1.0 \text{ GeV}^2$ , the DSEQCD approach failed to describe the CLAS results [5, 25, 27] on the  $\Delta(1232)3/2^+$  and  $N(1440)1/2^+$   $\gamma_v p N^*$  electrocouplings [31, 33].

Furthermore, most quark models [36–39] that take into account the contributions from quark degrees of freedom only, have substantial shortcomings in describing resonance electrocouplings at  $Q^2 < 1.0 \text{ GeV}^2$  even if they provide a reasonable description of the experimental results at higher photon virtualities. These are the indications for the contributions of degrees of freedom other than dressed quarks to the structure of excited nucleon states, contributions that become more relevant at small photon virtualities.

A successful description of the CLAS results on the  $N(1440)1/2^+$   $\gamma_v p N^*$  electrocouplings [5, 25, 27] has been recently achieved at small photon virtualities up to  $0.5 \text{ GeV}^2$  within the framework of effective field theory employing pions,  $\rho$  mesons, the nucleon, and the Roper  $N(1440)1/2^+$  resonance as the effective degrees

of freedom [40]. This success emphasizes the importance of meson-baryon degrees of freedom for the structure of excited nucleon states at small photon virtualities. Furthermore, a general unitarity requirement imposes meson-baryon contributions to both resonance electromagnetic excitations and hadronic decay amplitudes. Studies of meson-baryon dressing contributions to the  $\gamma_v p N^*$  electrocouplings from the global analysis of the  $N\pi$  photo-, electro-, and hadroproduction data carried out by Argonne-Osaka Collaboration [41–43] within the framework of a coupled channel approach, conclusively demonstrated the contributions from both meson-baryon and quark degrees of freedom to the structure of nucleon resonances.

Some quark models that have been developed [44–48] take into account the contribution from both meson-baryon and quark degrees of freedom to the structure of excited nucleon states. Implementation of meson-baryon degrees of freedom allowed for a considerably improved description of the CLAS results on the  $N(1440)1/2^+$  and  $N(1520)3/2^-$   $\gamma_v p N^*$  electrocouplings at photon virtualities  $Q^2 < 1.0 \text{ GeV}^2$ , while simultaneously retaining a good description of these results for  $Q^2 > 2.0 \text{ GeV}^2$ .

Physics analyses of the CLAS results [5, 25, 27] on the  $\gamma_v p N^*$  electrocouplings revealed the structure of excited nucleon states at photon virtualities  $Q^2 < 5.0 \text{ GeV}^2$  as a complex interplay between meson-baryon and quark degrees of freedom. The relative contributions from the meson-baryon cloud and the quark core are strongly dependent on the quantum numbers of the excited nucleons. Analyses of the  $A_{1/2}$  electrocouplings of the  $N(1520)3/2^-$  resonance [43, 49] demonstrated that this amplitude is dominated by quark core contributions in the entire range of  $Q^2 < 5.0 \text{ GeV}^2$  measured by CLAS. However, the recent analysis [44] of the first CLAS results [15] on the  $N(1675)5/2^-$   $\gamma_v p N^*$  electrocouplings suggested a dominance of the meson-baryon cloud. The experimental results on the  $\gamma_v p N^*$  electrocouplings for all prominent resonances obtained in a wide range of photon virtualities are of particular importance in order to explore the contributions from different degrees of freedom to the resonance structure.

Analyses of different exclusive channels are essential for a reliable extraction of the resonance parameters over the full spectrum of excited nucleon states. Currently the separation of the resonant and non-resonant parts of the electroproduction amplitudes can be done only within phenomenological reaction models. Therefore, the credibility of any resonance parameters extracted from the meson electroproduction data fit within the framework of any particular reaction model should be further examined. Non-resonant mechanisms in various meson-electroproduction channels are completely different, while the  $\gamma_v N N^*$  electrocouplings are the same. Consistent results for the  $\gamma_v p N^*$  electrocouplings of the  $N(1440)1/2^+$  and  $N(1520)3/2^-$  resonances that were determined from independent analyses of the major meson electroproduction channels,  $\pi^+n$ ,  $\pi^0p$ , and  $\pi^+\pi^-p$ ,

demonstrate that the extractions of these fundamental quantities are reliable as these different electroproduction channels have quite different backgrounds [27]. Furthermore, this consistency also strongly suggests that the reaction models [25–27] developed for the description of these channels will provide a reliable evaluation of the  $\gamma_v NN^*$  electrocouplings for analyzing either single- or charged double-pion electroproduction data. These models then make it possible to determine the electrocouplings for almost all well-established resonances that decay preferentially to the  $N\pi$  and/or  $N\pi\pi$  final states. The information on the  $\gamma_v NN^*$  electrocouplings available from the exclusive charged double-pion electroproduction off the proton is still rather limited and will be extended by the results of this paper.

In this paper we present the results on the electrocouplings of the  $N(1440)1/2^+$ ,  $N(1520)3/2^-$ , and  $\Delta(1620)1/2^-$  resonances at the photon virtualities  $0.5 \text{ GeV}^2 < Q^2 < 1.5 \text{ GeV}^2$ , obtained from the analysis of the CLAS data on  $\pi^+\pi^-p$  electroproduction off the proton [24]. The analysis was carried out employing the JM reaction model [26, 27], which has been further developed to provide a framework for the determination of the  $\gamma_v pN^*$  electrocouplings from a combined fit of unpolarized differential cross sections in a broader kinematic area of  $W$  and  $Q^2$  in comparison with that covered in our previous studies [26, 27]. This paper extends the available information on the  $N(1440)1/2^+$  and  $N(1520)3/2^-$  electrocouplings from the charged double-pion exclusive electroproduction off the proton and provides the first results on the electrocouplings and the hadronic decay widths of the  $\Delta(1620)1/2^-$  resonance to the  $\pi\Delta$  and  $\rho N$  final states.

The paper is organized as follows. In Section II we describe the JM reaction model employed for the extraction of the resonance parameters and the fitted experimental data. A special fitting procedure that allowed us to account for the experimental data and the reaction model uncertainties is presented in Section III. The results on the  $\gamma_v pN^*$  electrocouplings and the hadronic decays of the  $N(1440)1/2^+$ ,  $N(1520)3/2^-$ , and  $\Delta(1620)1/2^-$  resonances to the  $\pi\Delta$  and  $\rho N$  final states extracted from the CLAS data [24] are presented in Section IV. Insights into the non-perturbative strong interaction mechanisms offered by our results and their impact on hadron structure theory are discussed in Section V with summary and outlook in Section VI.

## II. ANALYSIS TOOLS FOR EVALUATION OF THE $\gamma_v pN^*$ RESONANCE ELECTROCOUPLINGS AND HADRONIC DECAY WIDTHS

The  $\gamma_v pN^*$  electrocouplings and hadronic decay widths of the  $N(1440)1/2^+$ ,  $N(1520)3/2^-$ , and  $\Delta(1620)1/2^-$  resonances to the  $\pi\Delta$  and  $\rho N$  final states were extracted from the fit of the CLAS charged double-pion electroproduction data [24] at  $W$  from 1.41 GeV to

1.66 GeV in three  $Q^2$ -bins centered at  $Q^2=0.65 \text{ GeV}^2$ ,  $0.95 \text{ GeV}^2$ , and  $1.3 \text{ GeV}^2$ . The JM meson-baryon model [26, 27] was employed for the description of the measured observables in the  $\gamma_v p \rightarrow \pi^+\pi^-p$  exclusive channel. This model was successfully used in our previous extraction of the  $N(1440)1/2^+$  and  $N(1520)3/2^-$  resonance electrocouplings at smaller  $Q^2 < 0.6 \text{ GeV}^2$  [27] from the CLAS charged double-pion electroproduction data [23] at  $W < 1.57 \text{ GeV}$ . In our current analysis of the CLAS  $\pi^+\pi^-p$  electroproduction data [24], the JM model was further developed in order to provide a data description in a wider area of  $W$  from 1.40 GeV to 1.82 GeV and at photon virtualities  $Q^2$  from  $0.5 \text{ GeV}^2$  to  $1.5 \text{ GeV}^2$ . In this section we describe the differential cross sections we fit for the resonance parameter extraction. We also present the basic features of the JM model relevant for the extraction of the  $\gamma_v pN^*$  electrocouplings from the data [24], focusing on the model updates needed to achieve a good description of the measured differential cross sections.

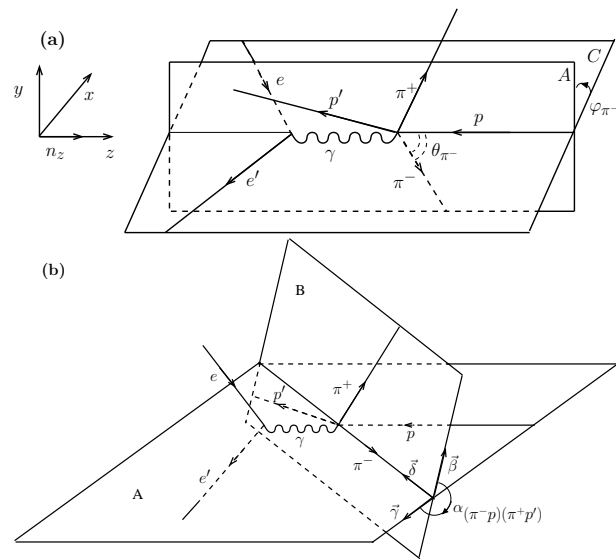


FIG. 1: Kinematic variables for the description of  $ep \rightarrow e'p'\pi^+\pi^-$  in the CM frame of the final-state hadrons corresponding to the explicit assignment presented in Section II A. Panel (a) shows the  $\pi^-$  spherical angles  $\theta_{\pi^-}$  and  $\varphi_{\pi^-}$ . Plane  $C$  represents the electron scattering plane. Plane  $A$  is defined by the 3-momenta of the initial state proton and the final state  $\pi^-$ . Panel (b) shows the angle  $\alpha_{[\pi^-p][\pi^+p']}$  between the two defined hadronic planes  $A$  and  $B$  or the plane  $B$  rotation angle around the axis aligned along the 3-momentum of the final  $\pi^-$ . Plane  $B$  is defined by the 3-momenta of the final state  $\pi^+$  and  $p'$ . The unit vectors  $\vec{\gamma}$  and  $\vec{\beta}$  are normal to the  $\pi^-$  three-momentum in the planes  $A$  and  $B$ , respectively.

$Q^2$ Intervals, GeV <sup>2</sup>	0.5-0.8
	0.65 central value
	0.8-1.1
	0.95 central value
$W$ Intervals, GeV covered in each $Q^2$ bin	1.1-1.5
	1.3 central value
	1.41-1.71
	13 bins

TABLE I: Kinematic area covered in the fit of the CLAS  $\pi^+\pi^-p$  electroproduction cross sections [24] for the extraction of the resonance parameters.

### A. Differential Cross Sections and Kinematic Variables

At a given invariant mass  $W$  and photon virtuality  $Q^2$ , the  $\gamma_{\nu}p \rightarrow \pi^+\pi^-p$  reaction can be fully described as a five-fold differential cross section  $d^5\sigma/d^5\tau$ , where  $d^5\tau$  is the differential of the five independent variables in the center-of-mass (CM) frame of the final  $\pi^+\pi^-p$  state. There are many possible choices [50] of the five independent variables. After defining  $M_{\pi^+p}$ ,  $M_{\pi^-p}$ , and  $M_{\pi^+\pi^-}$  as invariant mass variables of the three possible two-particle pairs in the  $\pi^+\pi^-p$  system, we adopt here the following assignment for the computation of the five-fold differential cross section:

$d^5\tau = dM_{\pi^+p}dM_{\pi^+\pi^-}d\Omega_{\pi^-}d\alpha_{[\pi^-p][\pi^+p']}$ , where  $\Omega_{\pi^-}$  ( $\theta_{\pi^-}$ ,  $\varphi_{\pi^-}$ ) are the final state  $\pi^-$  spherical angles with respect to the direction of the virtual photon with the  $\varphi_{\pi^-}$  defined as the angle between the hadronic plane A and the electron scattering plane C, see Fig 1 (a), and  $\alpha_{[\pi^-p][\pi^+p']}$  is the rotation angle of the plane B defined by the momenta of the final state  $\pi^+p'$  around the axis defined by the final state  $\pi^-$  momentum, see Fig. 1 (b).

All frame-dependent variables are defined in the final hadron CM frame. The relations between the momenta of the final-state hadrons and the aforementioned five variables can be found in Ref. [23].

The  $\pi^+\pi^-p$  electroproduction data have been collected in the bins of a seven-dimensional space. As mentioned above, five variables are needed to fully describe the final hadron kinematics, while to describe the initial state kinematics, two others variables,  $W$  and  $Q^2$ , are required. The huge number of seven dimensional bins over the reaction phase space ( $\approx 500,000$  bins) does not allow us to use the correlated multi-fold differential cross sections in the analysis of the data, where the statistics decrease drastically with increasing  $Q^2$ . More than half of the seven-dimensional phase-space bins of the final state hadrons are not populated due to statistical limitations. This is a serious obstacle for any analysis method that employs information on the behavior of multi-fold differential cross sections. We therefore use the following one-fold differential cross sections in each bin of  $W$  and  $Q^2$  covered by

One-fold differential cross section	Interval Covered	Number of Bins
$\frac{d\sigma}{dM_{\pi^+p}} (\mu\text{b}/\text{GeV})$	$M_{\pi^+p_{min}} - M_{\pi^+p_{max}}$	10
$\frac{d\sigma}{dM_{\pi^+\pi^-}} (\mu\text{b}/\text{GeV})$	$M_{\pi^+\pi^-_{min}} - M_{\pi^+\pi^-_{max}}$	10
$\frac{d\sigma}{dM_{\pi^-p}} (\mu\text{b}/\text{GeV})$	$M_{\pi^-p_{min}} - M_{\pi^-p_{max}}$	10
$\frac{d\sigma}{d(-\cos(\theta_{\pi^-}))} (\mu\text{b}/\text{rad})$	0-180°	10
$\frac{d\sigma}{d(-\cos(\theta_{\pi^+}))} (\mu\text{b}/\text{rad})$	0-180°	10
$\frac{d\sigma}{d(-\cos(\theta_{p'}))} (\mu\text{b}/\text{rad})$	0-180°	10
$d\sigma/d\alpha_{[\pi^-p][\pi^+p']}$ ( $\mu\text{b}/\text{rad}$ )	0-360°	5
$d\sigma/d\alpha_{[\pi^+p][\pi^-p']}$ ( $\mu\text{b}/\text{rad}$ )	0-360°	5
$d\sigma/d\alpha_{[\pi^+\pi^-][pp']}$ ( $\mu\text{b}/\text{rad}$ )	0-360°	5

TABLE II: List of the fit one-fold differential cross sections measured with CLAS [24] and the binning over the kinematic variables.  $M_{min_{i,j}} = M_i + M_j$ ,  $M_{max_{i,j}} = W - M_k$ , where  $M_{i,j}$  and  $M_k$  are the invariant masses of the final state hadron pair  $i,j$ , and the mass of the third final state hadron  $k$ , respectively.

the data:

- invariant mass distributions for the three pairs of the final state particles  $d\sigma/dM_{\pi^+\pi^-}$ ,  $d\sigma/dM_{\pi^+p}$ , and  $d\sigma/dM_{\pi^-p}$ ;
- angular distributions for the spherical angles of the three final state particles  $d\sigma/d(-\cos\theta_{\pi^-})$ ,  $d\sigma/d(-\cos\theta_{\pi^+})$ , and  $d\sigma/d(-\cos\theta_{p'})$  in the CM frame;
- angular distributions for the three  $\alpha$ -angles determined in the CM frame:  $d\sigma/d\alpha_{[\pi^-p][\pi^+p']}$ ,  $d\sigma/d\alpha_{[\pi^+p][\pi^-p']}$ , and  $d\sigma/d\alpha_{[\pi^+\pi^-][pp']}$ . The  $d\sigma/d\alpha_{[\pi^+p][\pi^-p']}$  and  $d\sigma/d\alpha_{[\pi^+\pi^-][pp']}$  differential cross sections are defined analogously to  $d\sigma/d\alpha_{[\pi^-p][\pi^+p']}$  describe above. More details on these observables can be found in Refs. [23, 27].

The one-fold differential cross sections were obtained by integrating the five-fold differential cross sections over the other four relevant kinematic variables of  $d^5\tau$ . However, the angular distributions for the spherical angles of the final state  $\pi^+$  and  $p$ , as well as for the rotation angles around the axes along the momenta of these final state hadrons, cannot be obtained with the aforementioned  $d^5\tau$ , since this differential does not depend on these variables. Two other sets of  $d^5\tau'$  and  $d^5\tau''$  differentials are required, which contain  $d\Omega_{\pi^+}d\alpha_{[\pi^+p][\pi^-p']}$  and  $d\Omega_{p'}d\alpha_{[pp'][\pi^+\pi^-]}$ , respectively, as described in Refs. [23, 26]. The five-fold differential cross sections evaluated over the other two  $d^5\tau'$  and  $d^5\tau''$  differentials were computed from the five-fold differential cross section over the  $d^5\tau$  differential detailed above by means of cross section interpolation. For each kinematic point in the five-dimensional phase space determined by the variables of the other two  $d^5\tau'$  and  $d^5\tau''$  differentials, the four-momenta of the three final state hadrons were computed, and from these values the five variables of the  $d^5\tau$  were

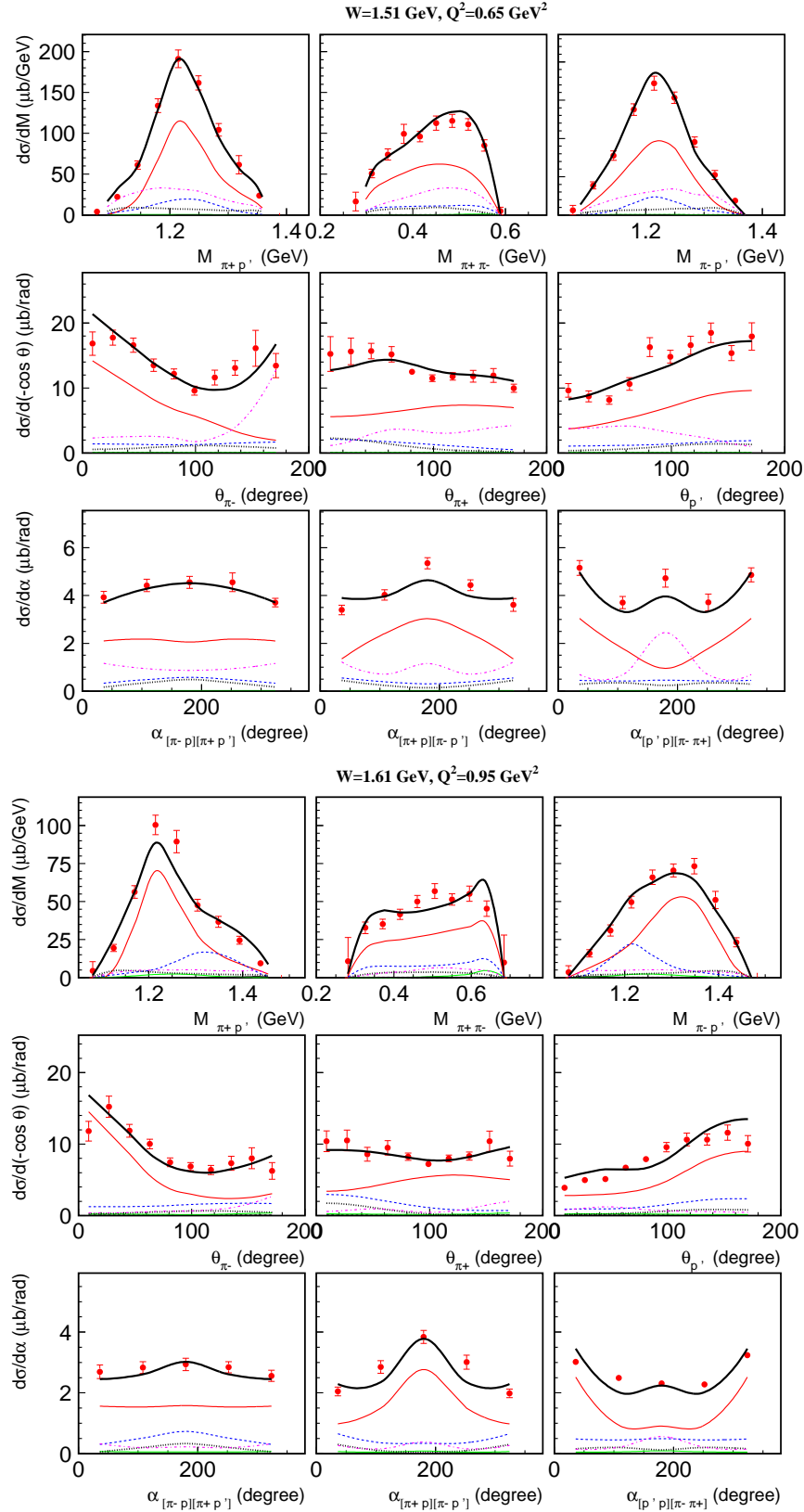


FIG. 2: (Color Online) Description of the CLAS  $ep \rightarrow e'p'\pi^+\pi^-$  data [24] within the framework of the JM model [26, 27] after implementation of the phases for the  $2\pi$  direct production mechanisms discussed in Section II B at  $W = 1.51 \text{ GeV}$ ,  $Q^2=0.65 \text{ GeV}^2$  (top) and at  $W = 1.61 \text{ GeV}$ ,  $Q^2=0.95 \text{ GeV}^2$  (bottom). Full model results are shown by the black thick solid lines together with the contributions from the isobar channels  $\pi^-\Delta^{++}$  (thin red lines),  $\pi^+\Delta^0$  (blue dash-dotted lines),  $\pi^+D_{13}^0(1520)$  (black dotted lines), and the  $2\pi$  direct production mechanisms (magenta dash-dotted lines). The contributions from other mechanisms described in Section II B are comparable with the data uncertainties and are not shown in the plot.

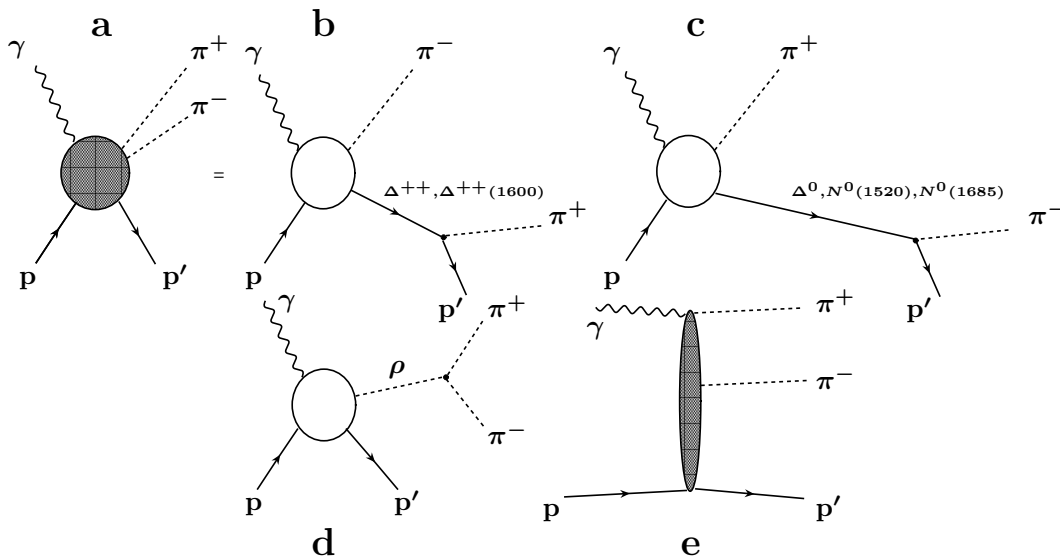


FIG. 3: The  $ep \rightarrow e'p'\pi^+\pi^-$  electroproduction mechanisms incorporated into the JM model [26, 27]: a) full amplitude; b)  $\pi^-\Delta^{++}$  and  $\pi^-\Delta^{++}(1600)\frac{3}{2}^+$  isobar channels; c)  $\pi^+\Delta^0$ ,  $\pi^+N^0(1520)\frac{3}{2}^-$ , and  $\pi^+N^0(1685)\frac{5}{2}^+$  isobar channels; d)  $\rho p$  meson-baryon channel; e) the  $2\pi$  direct electroproduction mechanisms.

determined. The  $d^5\sigma/d^5\tau$  cross sections were interpolated into this five-dimensional kinematic point. All details related to the evaluation of the nine one-fold differential cross sections from the CLAS data on  $\pi^+\pi^-p$  electroproduction off the proton can be found in Ref. [23].

An example of the data analyzed in two particular bins of  $W$  and  $Q^2$  is shown in Fig. 2. The kinematic area covered in our analysis and the data binning are summarized in Tables I and II.

### B. The Reaction Model for Extraction of the Resonance Parameters

A phenomenological analysis of the CLAS  $\pi^+\pi^-p$  electroproduction data [24] was carried out for  $W < 1.82$  GeV and at photon virtualities  $0.5 \text{ GeV}^2 < Q^2 < 1.5 \text{ GeV}^2$ . This work allows us to establish all essential mechanisms that contribute to the measured cross sections. The peaks in the invariant mass distributions provide evidence for the presence of the channels arising from  $\gamma_v p \rightarrow \text{Meson} + \text{Baryon} \rightarrow \pi^+\pi^-p$  having an unstable baryon or meson in the intermediate state. Pronounced dependencies in the angular distributions further allow us to establish the relevant  $t$ -,  $u$ -, and  $s$ -channel exchanges. The mechanisms without pronounced kinematic dependencies are identified through examination of various differential cross sections, with their presence emerging from the correlation patterns. The phenomenological reaction model JM [26, 27, 51, 52] was developed with the primary objective to determine the  $\gamma_v p N^*$  electrocouplings and the corresponding  $\pi\Delta$  and  $\rho N$  partial hadronic decay widths from fitting all measured observables in the  $\pi^+\pi^-p$  electroproduction channel. The relationships be-

tween the  $\pi^+\pi^-p$  electroproduction cross sections and the three-body production amplitudes employed in the JM model are given in Appendix D of Ref. [26].

The amplitudes of the  $\gamma_v p \rightarrow \pi^+\pi^-p$  reaction are described in the JM model as a superposition of the  $\pi^-\Delta^{++}$ ,  $\pi^+\Delta^0$ ,  $\rho p$ ,  $\pi^+D_{13}^0(1520)$ ,  $\pi^+F_{15}^0(1685)$ , and  $\pi^-\Delta^{++}(1600)$  sub-channels with subsequent decays of the unstable hadrons to the final  $\pi^+\pi^-p$  state, and additional direct  $2\pi$  production mechanisms, where the final  $\pi^+\pi^-p$  state comes about without going through the intermediate process of forming unstable hadron states. The mechanisms incorporated into the JM model are shown in Fig. 3.

The JM model incorporates contributions from all well-established  $N^*$  states with listed in Table III considering the resonant contributions only to  $\pi\Delta$  and  $\rho p$  sub-channels. We also have included the  $3/2^+(1720)$  candidate state, whose existence is suggested in the analysis [24] of the CLAS  $\pi^+\pi^-p$  electroproduction data. In the versions of the JM model beginning in 2012 [27], the resonant amplitudes are described by a unitarized Breit-Wigner ansatz as proposed in Ref. [53]; the model was modified to make it fully consistent with a relativistic Breit-Wigner parameterization of each individual  $N^*$  state contributions in the JM model [51] that also accounts for the energy-dependent resonance hadronic decay widths. A unitarized Breit-Wigner ansatz accounts for the transition between the same and different resonances in the dressed resonant propagator, which makes the resonant amplitudes consistent with restrictions imposed by a general unitarity condition [43, 54]. Quantum number conservation in the strong interaction allows for transitions between the pairs of  $N^*$  states  $N(1520)3/2^- \leftrightarrow N(1700)3/2^-$ ,  $N(1535)1/2^- \leftrightarrow$

$N(1650)1/2^-$ , and  $3/2^+(1720) \leftrightarrow N(1720)3/2^+$  incorporated into the JM model. We found that the use of the unitarized Breit-Wigner ansatz has a minor influence on the  $\gamma_v NN^*$  electrocouplings, but it may substantially affect the  $N^*$  hadronic decay widths determined from fits to the CLAS data.

The non-resonant contributions to the  $\pi\Delta$  sub-channels incorporate a minimal set of current-conserving Born terms [26, 51]. They consist of  $t$ -channel pion exchange,  $s$ -channel nucleon exchange,  $u$ -channel  $\Delta$  exchange, and contact terms. Non-resonant Born terms were reggeized and current conservation was preserved as proposed in Refs. [55, 56]. The initial- and final-state interactions in  $\pi\Delta$  electroproduction are treated in an absorptive approximation, with the absorptive coefficients estimated from the data from  $\pi N$  scattering [51]. Non-resonant contributions to the  $\pi\Delta$  sub-channels further include additional contact terms that have different Lorentz-invariant structures with respect to the contact terms in the sets of Born terms. These extra contact terms effectively account for non-resonant processes in the  $\pi\Delta$  sub-channels beyond the Born terms, as well as for the final-state interaction effects that are beyond those taken into account by the absorptive approximation. Parameterizations of the extra contact terms in the  $\pi\Delta$  sub-channels are given in Ref. [26]. A phenomenological treatment of the initial and final state interactions [51] along with the extra-contact-terms [26] in the  $\pi\Delta$  sub-channels determined from fits to the data are important in order to account for the constraints imposed by unitarity on the non-resonant amplitudes of these sub-channels.

The contributions from the  $\rho p$  meson-baryon channel are quite small in the range of  $W < 1.71$  GeV where the resonance parameters presented in this paper are determined. However, reliable accounting of this channel is important for ascertaining the electrocouplings and the corresponding hadronic parameters of the resonances in the aforementioned range of  $W$ . Non-resonant amplitudes in the  $\rho p$  sub-channel are described within the framework of a diffractive approximation, which also takes into account the effects caused by  $\rho$ -line shrinkage [57]. The latter effects play a significant role in near-threshold and sub-threshold  $\rho$ -meson production for  $W < 1.71$  GeV. The previous analyses of the CLAS data [23, 24] have revealed the presence of the  $\rho p$  sub-channel contributions for  $W > 1.5$  GeV.

The  $\pi^+ N^0(1520)3/2^-$ ,  $\pi^+ N^0(1685)5/2^+$ , and  $\pi^- \Delta(1600)3/2^+$  sub-channels are described in the JM model by non-resonant contributions only. The amplitudes of the  $\pi^+ N^0(1520)3/2^-$  sub-channel were derived from the non-resonant Born terms in the  $\pi\Delta$  sub-channels by implementing an additional  $\gamma_5$ -matrix that accounts for the opposite parities of  $\Delta(1232)3/2^+$  and  $N(1520)3/2^-$  [61]. The magnitudes of the  $\pi^+ N^0(1520)3/2^-$  production amplitudes were independently fit to the data for each bin in  $W$  and  $Q^2$ . The contributions from the  $\pi^+ N^0(1520)3/2^-$  sub-channel

$N^*$ states incorporated into the data fit	Mass, GeV	Total decay width $\Gamma_{tot}$ , GeV	BF $\pi\Delta$ , %	BF $\rho p$ , %	$N^*$ electro-coupling variation in the fit
$N(1440)1/2^+$	var	var	var	var	[60] var
$N(1520)3/2^-$	var	var	var	var	[60] var
$N(1535)1/2^-$	var	var	var	var	[25] fix
$\Delta(1620)1/2^-$	var	var	var	var	[52, 61] var
$N(1650)1/2^-$	var	var	var	var	[62] var
$N(1680)5/2^+$	1.68	0.12	12	5.5	[52, 61] var
$N(1700)3/2^-$	1.74	0.19	53	45	[52, 61] fix
$\Delta(1700)3/2^-$	1.70	0.26	89	2	[52, 61] fix
$3/2^+(1720)$	1.72	0.09	55	7	[5] fix
$N(1720)3/2^+$	1.73	0.11	47	36	[5] fix

TABLE III: List of resonances invoked in the  $\pi^+\pi^-p$  fit and their parameters: total decay widths  $\Gamma_{tot}$  and branching fractions (BF) to the  $\pi\Delta$  and  $\rho N$  final states. The quoted values for the hadronic parameters are taken from earlier fits [5, 52] to the CLAS  $\pi^+\pi^-p$  data [24]. The quantities labeled as *var* correspond to the variable parameters fit to the CLAS  $\pi^+\pi^-p$  data [24] within the framework of the current JM model version. Start values for the resonance electrocouplings are taken from the references listed in the last column and extrapolated to the  $Q^2$  area covered by the CLAS experiment [24].  $3/2^+(1720)$  represents the candidate  $N^*$  state with the signal reported in a previous analysis of CLAS data [24].

should be taken into account for  $W > 1.5$  GeV.

The  $\pi^+ N^0(1685)5/2^+$  and  $\pi^- \Delta^{++}(1600)3/2^+$  sub-channel contributions are seen in the data [24] at  $W > 1.6$  GeV. These contributions are almost negligible at smaller  $W$ . The effective contact terms were employed in the JM model for parameterization of these sub-channel amplitudes [61]. The magnitudes of the  $\pi^+ N^0(1685)5/2^+$  and  $\pi^- \Delta^{++}(1600)3/2^+$  sub-channel amplitudes were fit to the data for each bin in  $W$  and  $Q^2$ .

In general, unitarity requires the presence of so-called  $2\pi$  direct production mechanisms in the  $\pi^+\pi^-p$  electroproduction amplitudes, where the final  $\pi^+\pi^-p$  state is created without going through the intermediate step of forming unstable hadron states [54]. These  $2\pi$  direct production processes are beyond the aforementioned contributions from the two-body sub-channels.  $2\pi$  direct production amplitudes were established for the first time in the analysis of the CLAS  $\pi^+\pi^-p$  electroproduction data [26]. They are described in the JM model by a sequence of two exchanges in the  $t$  and/or  $u$  channels by unspecified particles that may come from two Regge trajectories. The amplitudes of the  $2\pi$  direct production mechanisms are parameterized by a Lorentz-invariant contraction between spin-tensors of the initial and final-state particles, while two exponential propagators describe the above-mentioned exchanges by unspecified particles. The magnitudes of these amplitudes are fit to the data for each bin in  $W$  and  $Q^2$ . The contributions from the  $2\pi$

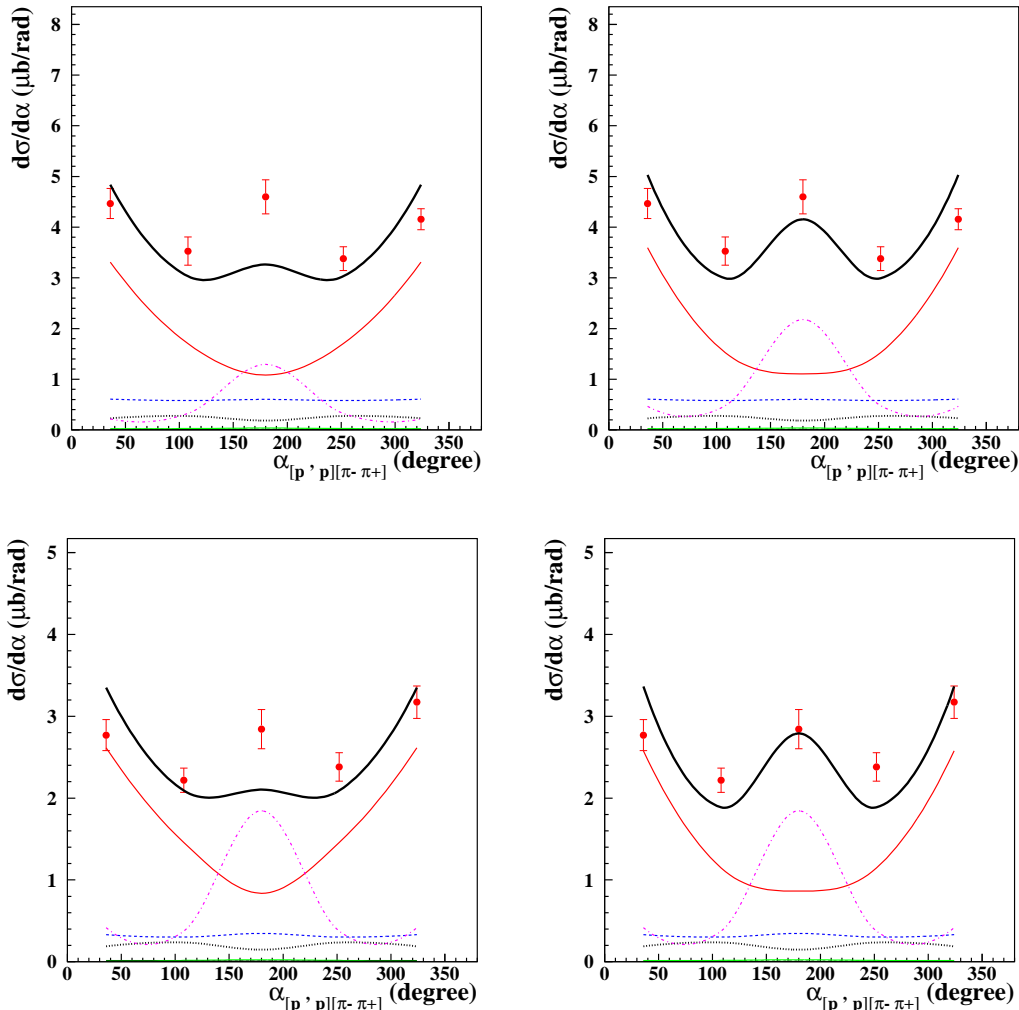


FIG. 4: (Color Online) Manifestation of the direct  $2\pi$  electroproduction mechanism relative phases in the CLAS data [24] on the angular distributions over the angle  $\alpha_{[\pi^+\pi^-][pp']}$ . The JM model results with the relative phases equal to zero are shown in the left column, while the computed cross sections with phases based on fits to the CLAS data [24] are shown in the right column. The sample plots shown are for  $W=1.56$  GeV,  $Q^2=0.65$  GeV<sup>2</sup> (top row) and  $W=1.54$  GeV,  $Q^2=0.95$  GeV<sup>2</sup> (bottom row). The curves for the different contributing meson-baryon channels are the same as those shown in Fig. 2.

direct production mechanisms are maximal and substantial ( $\approx 30\%$ ) for  $W < 1.5$  GeV and they decrease with increasing  $W$ , contributing less than 10% for  $W > 1.7$  GeV. However, even in this kinematic regime,  $2\pi$  direct production mechanisms can be seen in the  $\pi^+\pi^-p$  electroproduction cross sections due to an interference of the amplitudes with the two-body sub-channels. Explicit expressions for the above-mentioned  $2\pi$  direct production amplitudes can be found in Appendices A-C of Ref. [26]. We are planning to explore the possibility to replace this phenomenological ansatz by the  $B_5$  Veneziano model that was employed successfully in the studies of charged double-kaon photoproduction [63].

The studies of the final state hadron angular distributions over  $\alpha_i$  ( $i = [\pi^-p][\pi^+p']$ ,  $[\pi^+p][\pi^-p']$ ,  $[\pi^+\pi^-][pp']$ )

conclusively demonstrated the need to implement the relative phases for all  $2\pi$  direct production mechanisms included in the JM model. Figure 4 shows the comparison of the measured data [24] to the differential cross sections  $d\sigma/d\alpha_{[\pi^+\pi^-][pp']}$  computed within the framework of the JM model for values of the relative phases of the  $2\pi$  direct production mechanisms fit to the data and for values of these phases equal to zero. The computed cross sections, assuming zero phases for all  $2\pi$  direct production amplitudes, underestimate the measured  $d\sigma/d\alpha_{[\pi^+\pi^-][pp']}$  cross sections at  $\alpha_{[\pi^+\pi^-][pp']}$  around  $180^\circ$  (left panel in Fig. 4). This is a consequence of destructive interference of these contributions with the amplitudes of other relevant processes at  $Q^2=0.95$  GeV<sup>2</sup> and insufficient constructive interference at  $Q^2=0.65$  GeV<sup>2</sup>. Fits to the data phases of



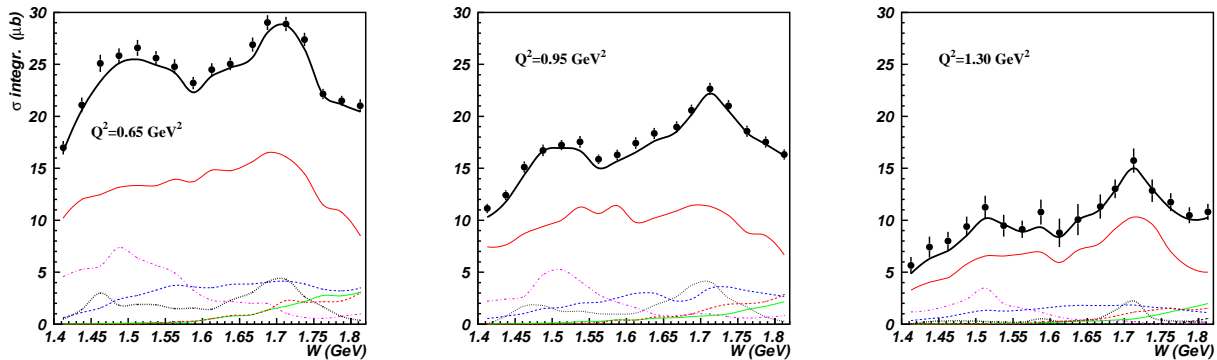


FIG. 5: (Color Online) Description of the fully integrated  $\pi^+\pi^-p$  electroproduction cross sections achieved within the framework of the updated JM model discussed in Section II B together with the cross sections for the various contributing mechanisms: full cross section (black solid),  $\pi^-\Delta^{++}$  (red thin solid),  $pp$  (green thin solid),  $\pi^+\Delta^0$  (blue thin dashed),  $\pi^+N^0(1520)3/2^-$  (black dotted), direct  $2\pi$  mechanisms (magenta thin dot-dashed), and  $\pi^+N^0(1685)5/2^+$  (red thin dashed). The data fits were carried out at  $W < 1.71$  GeV.

$2\pi$  direct production mechanisms change the interference pattern and allow us to improve the description of the  $d\sigma/d\alpha_{[\pi^+\pi^-][pp']}$  angular distributions at  $W > 1.48$  GeV in all three  $Q^2$ -bins under study, while retaining the same or even better quality of description of the other eight one-fold differential cross sections. Examples of the achieved improvements implementing the relative phases of the  $2\pi$  direct production mechanisms are shown in the right column of Fig. 4.

The JM model provides a reasonable description of the nine  $\pi^+\pi^-p$  one-fold differential cross sections for  $W < 1.8$  GeV and  $Q^2 < 1.5$  GeV<sup>2</sup>. As a typical example, the nine one-fold differential cross sections and their corresponding descriptions for  $W = 1.51$  GeV and  $Q^2 = 0.65$  GeV<sup>2</sup> and for  $W = 1.61$  GeV and  $Q^2 = 0.95$  GeV<sup>2</sup> are shown in Fig. 2, together with the contributions from each of the individual mechanisms incorporated into the JM model. Any contributing mechanism will be manifested by substantially different shapes in the cross sections for the observables, all of which are highly correlated through the underlying reaction dynamics. The simultaneous description of all the nine one-fold differential cross sections allows for identifying the essential mechanisms contributing to the  $\pi^+\pi^-p$  electroproduction off the proton.

Descriptions of the fully integrated  $\pi^+\pi^-p$  electroproduction cross sections are shown in Fig. 5 together with the contributions from the meson-baryon mechanisms of the JM model. The major part of the  $\pi^+\pi^-p$  electroproduction off the proton at  $W < 1.6$  GeV is due to contributions from the two  $\pi\Delta$  isobar channels,  $\pi^-\Delta^{++}$  and  $\pi^+\Delta^0$ . The  $\Delta^{++}(1232)$  resonance is clearly seen in all  $\pi^+p$  mass distributions for  $W > 1.4$  GeV, while contributions from the  $\pi^+\Delta^0$  isobar channel are needed to better describe the data in the low mass regions of the  $\pi^-p$  mass distributions. The strength of the  $\pi^-\Delta^{++}$  iso-

bar channel observed in the data [23, 24] is approximately nine times larger than that of  $\pi^+\Delta^0$  [26] due to isospin invariance. The CLAS data [24] demonstrated sub-leading but still important contributions from the  $\pi^+D_{13}^0(1520)$  meson-baryon channel. This contribution is needed for a description of the  $\pi^+$  CM-angular distributions at forward angles and allows us to better describe the  $\pi^-p$  invariant mass distributions as  $W$  increases (see Fig. 2). The contributions from  $2\pi$  direct production mechanisms shown in Fig. 5 were obtained with the phases of these mechanisms derived from the CLAS data [24]. These contributions are substantial, up to 30% at  $W < 1.5$  GeV. They decrease sharply as  $W$  increases. Direct  $2\pi$  production mechanisms become minor at  $W > 1.7$  GeV, but they still should be taken into account because of their interference with larger amplitudes of other contributing mechanisms.  $2\pi$  direct production mechanisms are kinematically allowed in the entire range of  $W$ , while meson-baryon channels with final mesons/baryons heavier than the pion/nucleon can be open at  $W$  larger than the respective threshold values. This may explain the biggest contributions from  $2\pi$  direct production mechanisms at small  $W < 1.5$  GeV. The  $\pi^+\pi^-p$  final state interaction with all open meson-baryon channels may be a plausible explanation for the sharp decrease of these mechanism contributions at  $W > 1.5$  GeV, see Fig 5. A quantitative description of this pronounced effect in the behavior of the  $2\pi$  direct production mechanisms represents a challenging task for the global multi-channel analysis of exclusive meson electroproduction within the framework of the coupled channel approaches under development by the Argonne-Osaka group [41, 58].

Accounting for the restrictions imposed by unitarity on the  $\pi^+\pi^-p$  electroproduction amplitudes represents an important requirement for reliable extraction of the resonance parameters. However, a rigorous implementa-

tion of unitarity for this three-body exclusive channel is still far from the reach of reaction theory and is outside the scope of this paper. To our knowledge, none of the available models is capable of providing fully unitarized amplitudes to fit the  $\pi^+\pi^-p$  data to determine the electroproduction amplitudes. A very promising step in this direction was made by the Argonne-Osaka group [59, 64]. Nevertheless, their approach is still under development. In this paper we employ a strategy that allows us to account phenomenologically for unitarity constraints in extracting the resonance parameters. As was mentioned above, we incorporated several features in the JM model in order to account for the unitarity restrictions on the resonant/non-resonant  $\pi^+\pi^-p$  electroproduction amplitudes: a) the unitarized Breit-Wigner ansatz for the resonant amplitudes, b) the phenomenological treatment of the initial and final state interactions and the inclusion of the extra contact terms for the non-resonant amplitudes of the  $\pi\Delta$  sub-channels, and c) direct  $2\pi$  production mechanisms. A good description of the nine one-fold differential cross sections in the entire kinematic area of  $W$  and  $Q^2$  analyzed in this paper strongly suggests a reliable parameterization of the squared  $\pi^+\pi^-p$  electroproduction amplitudes achieved for the CLAS data [24] fit within the framework of the JM model updated as was described in earlier. The  $\pi^+\pi^-p$  electroproduction amplitudes determined from a fit to the data account for the restrictions imposed by unitarity on their magnitudes at the real energy axis because the measured differential cross sections should be consistent with the unitarity constraints. The resonant contributions to the differential cross sections were obtained from these amplitudes switching off the non-resonant parts. In Section III we will discuss in detail the extraction of the resonant contributions to the differential cross sections. The resonant parameters were extracted from the resonant contributions to the differential cross sections employing the unitarized Breit-Wigner ansatz for the resonant amplitudes. Therefore, the unitarity constraints on the resonant amplitudes were fully taken into account. The resonant parameters were obtained at the real energy axis at the resonant point  $W = M_{N^*}$ . The reliability of the resonance parameters obtained in this way is determined by credible isolation of the resonant contributions to the differential cross sections, which will be discussed in Section III.

### III. THE CLAS DATA FIT

The resonance parameters obtained in our work were determined in the simultaneous fit to the CLAS  $\pi^+\pi^-p$  electroproduction differential cross sections [24] in the three  $Q^2$ -bins listed in Table I. The  $W$ -area included in the fit is limited to  $W < 1.71$  GeV. Currently the resonance content for the structure in the  $W$ -dependence of the fully integrated  $\pi^+\pi^-p$  cross sections at  $W \approx 1.7$  GeV [24] is still under study [65]. For this reason the resonance parameters for the states located at  $W$  above

Variable parameters	Ranges covered in variations of the start parameters, % from their values
Magnitude of the additional contact term amplitude in the $\pi^-\Delta^{++}$ sub-channel	40.0
Magnitude of the additional contact term amplitude in the $\pi^+\Delta^0$ sub-channel	45.0
Magnitude of the $\pi^+N^0(1520)3/2^-$ amplitude	45.0
Magnitudes of the six $2\pi$ direct production amplitudes	20.0-30.0

TABLE IV: Variable parameters of the non-resonant mechanisms incorporated into the JM model [26, 27]. The ranges in the table correspond to the  $3\sigma$  areas around the start values of the parameters.

1.64 GeV are outside of this paper scope.

In order to provide a realistic evaluation of the resonance parameters, we abandoned the traditional least-squares fit, since the parameters extracted in such a fit correspond to a single presumed global minimum, while the experimental data description achieved with other local minima may be equally good within the data uncertainties. Furthermore, the traditional evaluation of the fit-parameter uncertainties, based on the error propagation matrix, cannot be used for the same reason.

The special data fit procedure described in Ref. [27] was employed for extraction of the resonance parameters. It allows us to obtain not only the best fit, but also to establish bands of the computed cross sections that are compatible with the data within their uncertainties. In the fit we simultaneously vary the resonant and non-resonant parameters of the JM model given in Tables III and IV, respectively. More details on the non-resonant mechanisms listed in Table IV can be found in Refs. [26, 27]. These non-resonant mechanisms have an essential influence on the data description at  $W < 1.71$  GeV. The values of the aforementioned non-resonant/resonant parameters were evaluated under simultaneous variation of:

- the magnitudes of additional contact-term amplitudes in the  $\pi^-\Delta^{++}$  and  $\pi^+\Delta^0$  isobar channels (2 parameters per  $Q^2$ -bin);
- the magnitudes of the  $\pi^+N^0(1520)3/2^-$  isobar channel (1 parameter per  $Q^2$ -bin);
- the magnitudes of all direct  $2\pi$  production amplitudes (9 parameters per  $Q^2$ -bin including the phases described in the Section II B);
- and the variable resonant parameters listed in Table III. The CLAS  $\pi^+\pi^-p$  data [24] at  $W <$

Resonances	$Q_{cent.}^2=0.65$ GeV <sup>2</sup>	$Q_{cent.}^2=0.95$ GeV <sup>2</sup>	$Q_{cent.}^2=1.30$ GeV <sup>2</sup>
$N(1440)1/2^+$	40	30	40
$N(1520)3/2^-$	20	20	30
$\Delta(1620)1/2^-$	40	40	40
$N(1650)1/2^-$	40	40	50

TABLE V:  $\sigma$  parameters employed in the variation of the resonance electrocouplings in % of their start values. The  $\sigma$  parameters listed for the  $\Delta(1620)1/2^-$  were applied as a variation of the  $S_{1/2}(Q^2)$  electrocouplings only. The variation of the  $A_{1/2}(Q^2)$  electrocouplings of this state is described in Section IV.

1.71 GeV are mostly sensitive to the variable electrocouplings of the  $N(1440)1/2^+$ ,  $N(1520)3/2^-$ ,  $\Delta(1620)1/2^-$ , and  $N(1650)1/2^-$  states (9 resonance electrocouplings per  $Q^2$ -bin), as well as the  $\pi\Delta$  and  $\rho p$  hadronic decay widths of these four resonances and of the  $N(1535)1/2^-$  state (12 parameters that remain the same in the entire kinematic area covered by the fit).

All of the aforementioned parameters are sampled around their start values, employing unrestricted normal distributions. In this way we mostly explore the range of  $\approx 3\sigma$  around the start parameter values. The  $W$ -dependencies of the magnitudes of the amplitudes of all non-resonant contributions are determined by adjusting their values to reproduce the measured nine one-fold differential charged double-pion electroproduction cross sections [24]. We apply multiplicative factors to the magnitudes of all non-resonant amplitudes. They remain the same in the entire  $W$ -interval covered by the fit within any  $Q^2$ -bin, but they depend on the photon virtuality  $Q^2$  and are fit to the data in each  $Q^2$ -bin independently. The multiplicative factors are varied around unity employing normal distributions with the  $\sigma$  values in the ranges listed in Table IV. In this way we retain the smooth  $W$ -dependencies of the non-resonant contributions established in the adjustment to the data and explore the possibility to improve the data description in the simultaneous variation of the resonant and non-resonant parameters.

In this fit we also vary the  $\gamma_v p N^*$  electrocouplings and the  $\pi\Delta$  and  $\rho p$  hadronic partial decay widths of the  $N(1440)1/2^+$ ,  $N(1520)3/2^-$ , and  $\Delta(1620)1/2^-$  resonances around their start values. The start values of the  $N(1440)1/2^+$  and  $N(1520)3/2^-$  electrocouplings were determined by interpolating the results from the analyses [25, 27] of the CLAS data on  $N\pi$  and  $\pi^+\pi^-p$  electroproduction off the proton in the range  $0.5 \text{ GeV}^2 < Q^2 < 1.5 \text{ GeV}^2$ . The electrocouplings of the  $N(1440)1/2^+$  and  $N(1520)3/2^-$  resonances were varied employing normal distributions with the  $\sigma$  parameters listed in Table V in terms of % of their start values. There were no restrictions on the minimum or maximum trial electrocoupling values, allowing us to mostly explore the area of  $\approx 3\sigma$

$N^*$ states	Mass, MeV	Total decay width, $\Gamma_{tot}$ , MeV
$N(1440)1/2^+$	1430-1480	200-450
$N(1520)3/2^-$	1515-1530	100-150
$N(1535)1/2^-$	1510-1560	100-200
$\Delta(1620)1/2^-$	1600-1660	130-160
$N(1650)1/2^-$	1640-1670	140-190

TABLE VI: The ranges of the resonance masses and total  $N^*$  hadronic decay widths employed to constrain the variation of their partial hadronic decay widths to the  $\pi\Delta$  and  $\rho N$  final states in the fit of the CLAS  $\pi^+\pi^-p$  electroproduction data [24].

around their start values.

The  $\pi^+\pi^-p$  electroproduction channel also has some sensitivity to the  $N(1535)1/2^-$  state, which couples dominantly to the  $N\pi$  and  $N\eta$  final states. The  $N(1535)1/2^-$  electrocouplings were taken from the CLAS analysis of  $N\pi$  electroproduction [25] and varied strictly inside the uncertainties reported in that paper.

The start values of the  $\Delta(1620)1/2^-$  and  $N(1650)1/2^-$  electrocouplings were taken from a preliminary analysis [5]. In this study the resonance electrocouplings were adjusted to describe the nine  $\pi^+\pi^-p$  one-fold differential cross sections [24] in the  $W$ -interval from 1.41 to 1.80 GeV and at  $0.5 \text{ GeV}^2 < Q^2 < 1.5 \text{ GeV}^2$ . However, the results [5] do not allow us to draw unambiguous conclusions regarding the resonant content of the structure at  $W \approx 1.7 \text{ GeV}$ . Therefore, we are using the results of this analysis as an estimate for the resonance electrocoupling start points to fit the charged double-pion electroproduction data [24] for  $W < 1.71 \text{ GeV}$  and  $0.5 \text{ GeV}^2 < Q^2 < 1.5 \text{ GeV}^2$ .

Since the resonance content of the structure at  $W \approx 1.7 \text{ GeV}$  is still under study, we present in this paper the fit results for the resonances with masses less than 1.64 GeV. In the extraction of these resonance parameters we also account for the contributions of the tails from several excited proton states in the third resonance region,  $N(1685)5/2^+$ ,  $N(1720)3/2^+$ , and  $\Delta(1700)3/2^-$ , with their start electrocoupling values taken from the analyses of Refs. [5, 66] and varied within 15% of their parameters. The  $N(1685)5/2^+$  state decays mostly to the  $N\pi$  final states. The electrocouplings of this state determined in the analyses of  $\pi^+\pi^-p$  electroproduction [5, 66] are consistent with the results of independent analysis of  $N\pi$  electroproduction [67]. This suggests a reasonable evaluation of the aforementioned third resonance region state electrocouplings in the analyses [5, 66] of the  $\pi^+\pi^-p$  electroproduction data as the start values for extraction of the resonance parameters for the states with masses less than 1.65 GeV. The contributions from the tails of the  $N(1675)5/2^-$ ,  $N(1700)1/2^+$ , and  $N(1700)3/2^-$  resonances were found to be negligible for  $W < 1.64 \text{ GeV}$ .

The  $\pi\Delta$  and  $\rho p$  hadronic decay widths of the  $N(1440)1/2^+$ ,  $N(1520)3/2^-$ , and  $N(1535)1/2^-$  reso-

$W$ intervals, GeV	$\chi^2/d.p.$ intervals for selected computed $\pi^+\pi^-p$ cross sections
1.41-1.51	2.12-2.30
1.46-1.55	2.27-2.60
1.51-1.61	2.55-2.85
1.56-1.66	2.63-2.72
1.61-1.71	2.49-2.68

TABLE VII: Quality of the fit of the CLAS data [24] on  $\pi^+\pi^-p$  electroproduction off the proton within the framework of the updated JM model described in Section II B. The resonance parameters are determined from the data fit at  $W < 1.71$  GeV.

nances were varied around their start values taken from previous analyses of the CLAS double-pion electroproduction data [27]. For the  $\Delta(1620)1/2^-$  state, the start values of these parameters were computed as the products of the  $N^*$  total decay widths from Ref. [68] and the branching fractions for decays to the  $\pi\Delta$  and  $\rho N$  final states were taken from analyses of  $\pi N \rightarrow \pi\pi N$  hadroproduction [69]. The ranges for the variations of the  $\pi\Delta$  and  $\rho p$  hadronic decay widths were restricted by the total  $N^*$  decay widths and their uncertainties shown in Table VI. The total  $N^*$  decay widths were obtained by summing the partial widths over all decay channels. The partial hadronic decay widths to all final states other than  $\pi\Delta$  and  $\rho p$  were computed as the products of RPP [68] values of the  $N^*$  total decay widths and branching fractions for decays to particular hadronic final states, which were taken from the analysis of Ref. [69]. We varied the  $\pi\Delta$  and  $\rho p$  hadronic decay widths of the  $N(1440)1/2^+$ ,  $N(1520)3/2^-$ ,  $N(1535)1/2^-$ ,  $\Delta(1620)1/2^-$ , and  $N(1650)1/2^-$  resonances simultaneously with their masses, keeping the hadronic  $N^*$  parameters independent of  $Q^2$ . The  $\pi\Delta$  and  $\rho p$  hadronic decay widths of all other resonances obtained in the analyses of Refs. [5, 66] and noted in Table III as “fix” were kept unchanged.

For each trial set of the JM model resonant and non-resonant parameters we computed nine one-fold differential  $\pi^+\pi^-p$  cross sections and the  $\chi^2$  per data point values ( $\chi^2/d.p.$ ). The  $\chi^2/d.p.$  values were estimated in point-by-point comparisons between the measured and computed one-fold differential cross sections in all bins of  $W$  from 1.41 GeV to 1.71 GeV and in the three  $Q^2$ -bins covered by the CLAS  $\pi^+\pi^-p$  data [24]. In the fit we selected the computed one-fold differential cross sections closest to the data with  $\chi^2/d.p.$  less than a predetermined maximum value  $\chi_{max}^2/d.p.$ . The values of  $\chi_{max}^2/d.p.$  were obtained by requiring that the computed cross sections with smaller  $\chi^2/d.p.$  be within the data uncertainties for the majority of the data points, based on point-by-point comparisons between the measured and the computed cross sections, see examples in Fig. 6, 7. In this fit procedure we obtained the  $\chi^2/d.p.$  intervals within which the computed cross sections described the data equally well within the data uncertainties.

We fit the CLAS data [24] consisting of nine one-fold differential cross sections of the  $ep \rightarrow e'p'\pi^+\pi^-$  electroproduction reaction in all bins of  $W$  and  $Q^2$  in the kinematic regions of  $W$ : 1.41 GeV  $< W < 1.51$  GeV, 1.46 GeV  $< W < 1.56$  GeV, 1.51 GeV  $< W < 1.61$  GeV, 1.56 GeV  $< W < 1.66$  GeV, 1.61 GeV  $< W < 1.71$  GeV and  $0.5 \text{ GeV}^2 < Q^2 < 1.5 \text{ GeV}^2$  within the framework of the fit procedure described above. The five intervals of  $W$  listed in Table VII were fit independently. Each of the aforementioned  $W$  intervals contained 375 fit data points. The  $\chi^2/d.p.$  intervals that correspond to an equally good data description within the data uncertainties are shown in Table VII. Their values demonstrate the quality of the CLAS  $\pi^+\pi^-p$  data description achieved in the fits. Examining the description of the nine one-fold differential cross sections, we found that the  $\chi^2/d.p.$  values were determined mostly by the deviations of only a few experimental data points from the computed fit cross sections. There were no discrepancies in describing the shapes of the differential cross sections, which would manifest themselves systematically in neighboring bins of  $W$  and  $Q^2$ . Typical fit examples for  $W=1.51$  GeV and neighboring  $Q^2$  intervals centered at 0.65 GeV<sup>2</sup> and 0.95 GeV<sup>2</sup>, as well as for  $W=1.61$  GeV and  $Q^2$  intervals centered at 0.95 GeV<sup>2</sup> and 1.30 GeV<sup>2</sup>, are shown in Fig. 6, 7.

Since only statistical data uncertainties were used in the computation of the  $\chi^2/d.p.$  values listed in Table VII, we concluded that a reasonable data description was achieved. The  $\chi^2/d.p.$  values of our fits are comparable with those obtained in the fit of the CLAS  $N\pi$  and  $\pi^+\pi^-p$  electroproduction data published in Refs. [15, 25] and in Ref. [27], respectively.

For each computed cross section point the resonant/non-resonant contributions were estimated switching off the non-resonant/resonant amplitudes, respectively. The determined resonant/non-resonant contributions to the nine one-fold differential cross sections are shown in Fig. 6, 7. The results suggest the unambiguous and credible separation between the resonant/non-resonant contributions achieved fitting the CLAS data [24] within the framework of the JM model. The determined resonant/non-resonant contributions are located within well defined ranges (see Fig. 6, 7) and show no evidence for separation ambiguities, which would manifest themselves as substantial differences between the particular computed resonant/non-resonant cross sections and the ranges determined for the resonant/non-resonant contributions as shown in Fig. 6, 7. Such features in the behavior of the resonant/non-resonant contributions remain unseen in the entire area of  $W$  and  $Q^2$  covered by our analysis. Furthermore, the uncertainties of the resonant/non-resonant contributions are comparable with the uncertainties of the measured cross sections, demonstrating again unambiguous resonant/non-resonant separation of a good accuracy. The credible isolation of the resonant contributions makes it possible to determine the resonance parameters from the resonant contributions

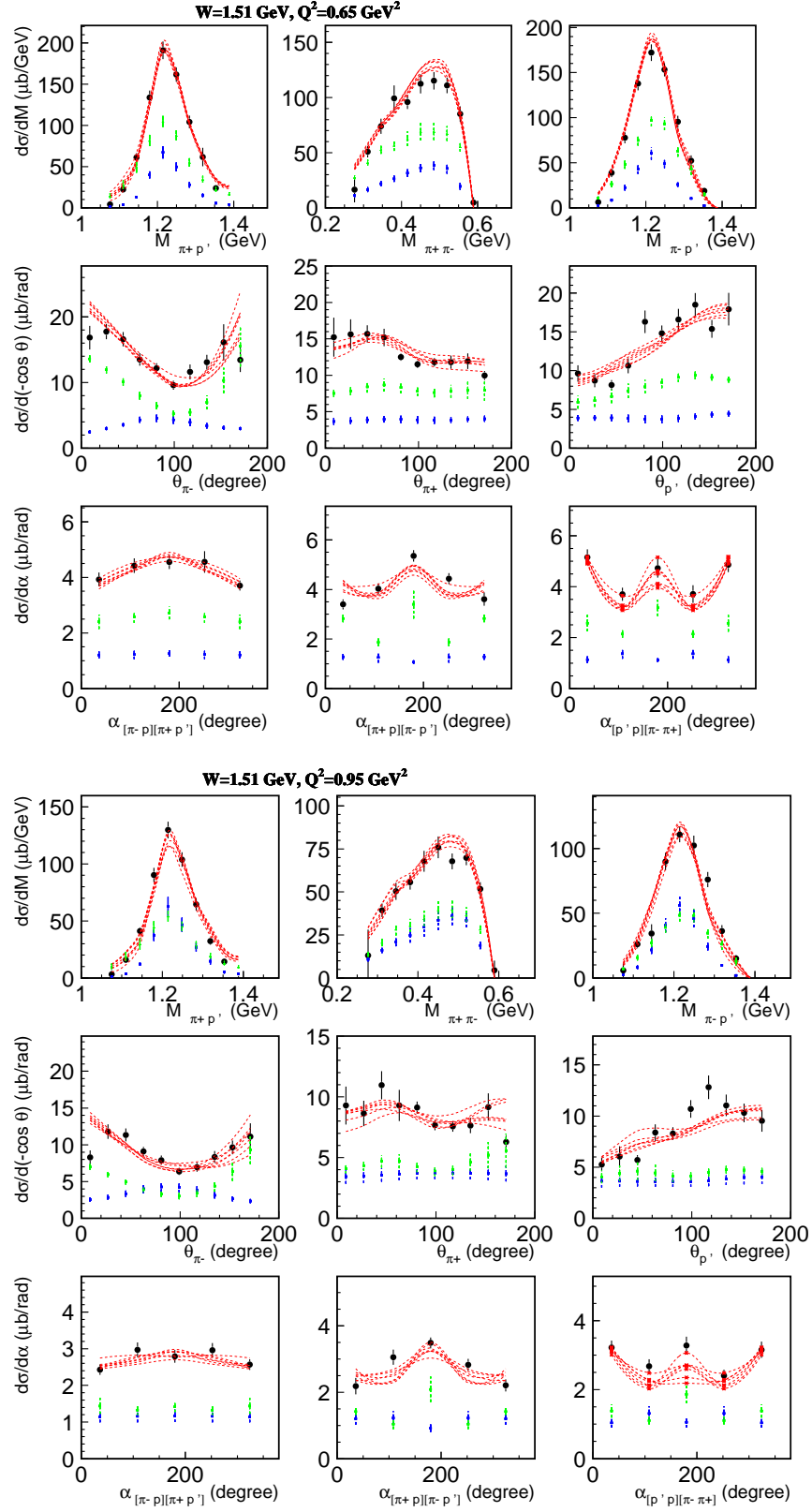


FIG. 6: (Color Online) Examples of fits to the CLAS data [24] on the nine one-fold differential  $\pi^+\pi^-p$  electroproduction cross sections in particular bins of  $W$  and  $Q^2$  within the framework of the updated JM model described in Section II B. The curves correspond to those fits with  $\chi^2/d.p.$  within the intervals listed in Table VII. The resonant and non-resonant contributions determined from the data fit within the framework of the JM15 model are shown by blue triangles and green squares, respectively.

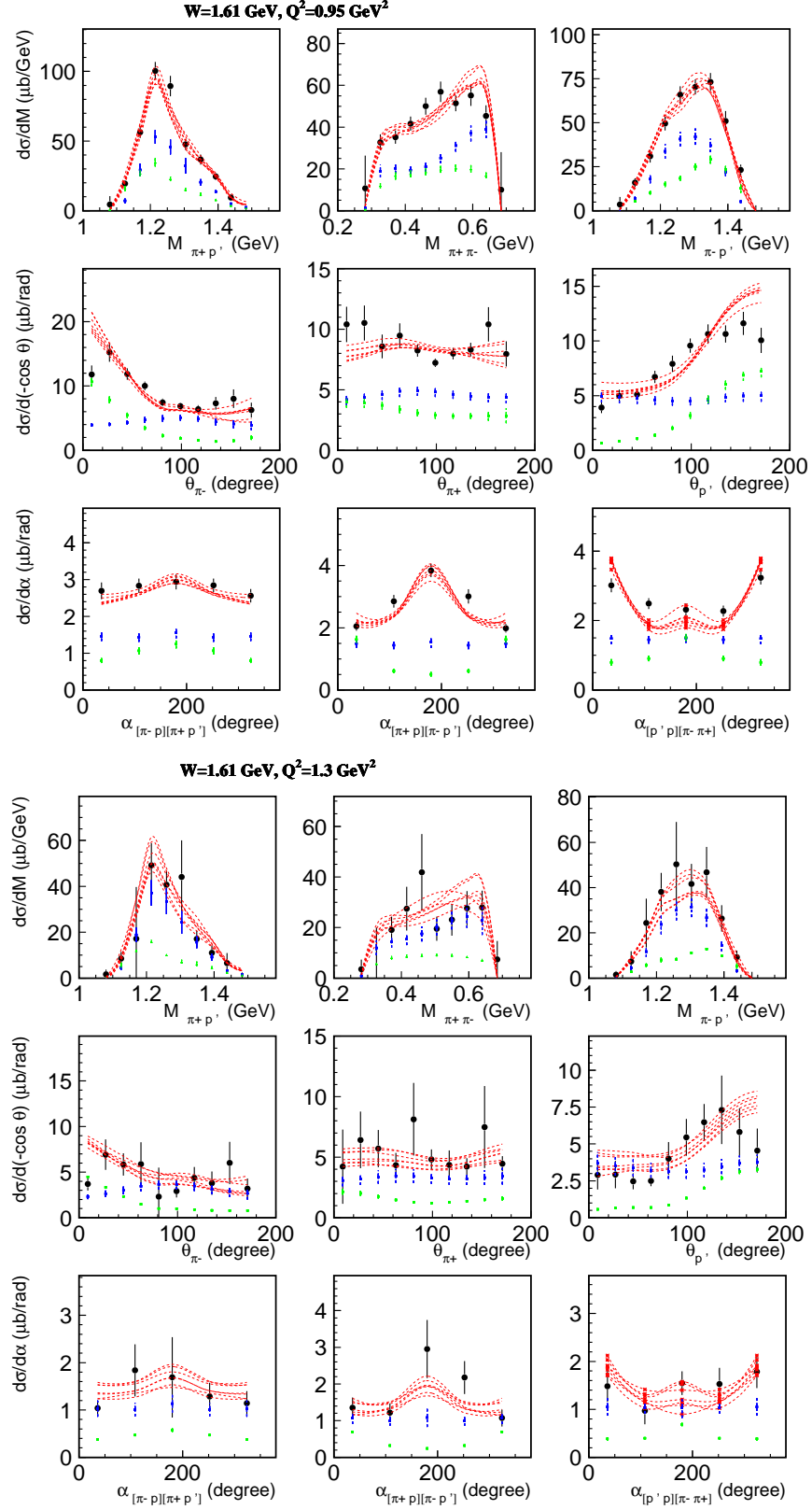


FIG. 7: (Color Online) The same as in Fig. 6, but in other bins of  $W$  and  $Q^2$ .

employing for their description the amplitudes of the unitarized Breit-Wigner ansatz that fully accounts for the unitarity restrictions on the resonant amplitudes.

The resonance parameters obtained from each of these equally good fits were averaged and their mean values were taken as the resonance parameters extracted from the data. The dispersions in these parameters were taken as the uncertainties. The resonance electrocoupling uncertainties obtained in this manner are shown in Figs. 8, 9, 10. Our fitting procedure allowed us to obtain more realistic uncertainties that take into account both statistical uncertainties in the data and systematic uncertainties imposed by the use of the JM reaction model. Furthermore, we consistently account for the correlations between variations of the non-resonant and resonant contributions while extracting the resonance parameters.

#### IV. EVALUATION OF THE $\gamma_v p N^*$ RESONANCE ELECTROCOUPLINGS AND HADRONIC DECAY WIDTHS TO THE $\pi\Delta$ AND $\rho N$ FINAL STATES

The procedure described in Section III allowed us to determine the  $\gamma_v p N^*$  electrocouplings of the  $N(1440)1/2^+$ ,  $N(1520)3/2^-$ , and  $\Delta(1620)1/2^-$  resonances and their uncertainties. Our analysis extended the information on the electrocouplings of the  $N(1440)1/2^+$  and  $N(1520)3/2^-$  states providing the first results in the range of photon virtualities  $0.5 \text{ GeV}^2 < Q^2 < 1.5 \text{ GeV}^2$  from the CLAS data. The  $\Delta(1620)1/2^-$  resonance decays preferentially to the  $N\pi\pi$  final state, making the charged double-pion electroproduction channel the major source of information on the electrocouplings of this state. Our studies provide the first results on the electrocouplings and hadronic decays of this resonance to the  $\pi\Delta$  and  $\rho p$  final states from analysis of exclusive charged double-pion electroproduction.

A special approach was developed for the evaluation of the  $\Delta(1620)1/2^-$  electrocouplings. The analysis of the CLAS  $\pi^+\pi^-p$  electroproduction data revealed that the  $A_{1/2}$  electrocoupling of this resonance was much smaller than the  $S_{1/2}$  for  $0.5 \text{ GeV}^2 < Q^2 < 1.5 \text{ GeV}^2$  [5]. The  $A_{1/2}$  variations computed as a percentage of the start value became too small. For realistic uncertainty estimates we varied  $A_{1/2}$  in a much wider range that made its tested absolute values comparable with those for the  $S_{1/2}$  electrocoupling. We fit the CLAS data [24] on  $\pi^+\pi^-p$  electroproduction by varying  $A_{1/2}$ , as described above, keeping the variation of all other resonant and non-resonant parameters as described in Section III.

In order to compare our results on the  $N(1440)1/2^+$  and  $N(1520)3/2^-$  electrocouplings in the  $\pi^+\pi^-p$  electroproduction channel with their values from the analysis of  $N\pi$  electroproduction, we must use in both of the exclusive electroproduction channels common branching fractions for the decays of these resonances to the  $N\pi$  and  $N\pi\pi$  final states. According to the RPP [68], the sum of

the branching fractions into the  $N\pi$  and  $N\pi\pi$  final states accounts for almost 100% of the total decay widths of the  $N(1440)1/2^+$  and  $N(1520)3/2^-$  states. Since the  $N\pi$  exclusive electroproduction channels are most sensitive to contributions from the  $N(1440)1/2^+$  and  $N(1520)3/2^-$  resonances, we re-evaluated the branching fraction for decay to the  $N\pi\pi$  final states  $BF(N\pi\pi)_{corr}$  as:

$$BF(N\pi\pi)_{corr} = 1 - BF(N\pi). \quad (1)$$

For these resonance decays to the  $N\pi\pi$  final states it turns out that the estimated branching fractions  $BF(N\pi\pi)_{corr}$  from Eq.(1) are slightly ( $<10\%$ ) different with respect to those obtained from the  $\pi^+\pi^-p$  fit ( $BF(N\pi\pi)_0$ ). Therefore, we multiplied the  $\pi\Delta$  and  $\rho p$  hadronic decay widths of the  $N(1440)1/2^+$  and  $N(1520)3/2^-$  from the  $\pi^+\pi^-p$  fit by the ratio  $\frac{BF(N\pi\pi)_{corr}}{BF(N\pi\pi)_0}$ . The  $N(1440)1/2^+$  and  $N(1520)3/2^-$  electrocouplings obtained in our analysis were then multiplied by the correction factors

$$C_{hd} = \sqrt{\frac{BF(N\pi\pi)_0}{BF(N\pi\pi)_{corr}}} \quad (2)$$

in order to keep the resonant parts and the computed differential  $\pi^+\pi^-p$  cross sections unchanged under the re-scaling of the resonance hadronic decay parameters described above.

The electrocouplings of the  $N(1440)1/2^+$ ,  $N(1520)3/2^-$ , and  $\Delta(1620)1/2^-$  resonances were determined in our analysis for  $0.5 \text{ GeV}^2 < Q^2 < 1.5 \text{ GeV}^2$ , where there is still no data on observables of other exclusive meson electroproduction channels measured with CLAS. We have developed special procedures to test the reliability of the resonance  $\gamma_v p N^*$  electrocouplings and their  $\pi\Delta$  and  $\rho p$  partial hadronic decay widths extracted from the charged double pion electroproduction data only. In order to check the reliability of the extracted  $\gamma_v p N^*$  electrocouplings, we carried out the extraction of the resonance parameters of all of the aforementioned resonances independently, fitting the CLAS  $\pi^+\pi^-p$  electroproduction data [24] in the five overlapping intervals of  $W$  given in Table VII covering in each fit the three  $Q^2$ -bins centered at  $0.65 \text{ GeV}^2$ ,  $0.95 \text{ GeV}^2$ , and  $1.30 \text{ GeV}^2$ . The non-resonant amplitudes in each of the aforementioned  $W$ -intervals are different, while the resonance parameters should remain the same as they are determined from the data fit in different  $W$ -intervals. The  $N(1440)1/2^+$ ,  $N(1520)3/2^-$ , and  $\Delta(1620)1/2^-$  state electrocouplings extracted in the fit of the  $\pi^+\pi^-p$  CLAS data [24] in the different  $W$ -intervals are shown in Figs. 8, 9, and 10.

The values of the  $N(1440)1/2^+$  and  $N(1520)3/2^-$  electrocouplings, as well as the  $S_{1/2}$  electrocoupling of the  $\Delta(1620)1/2^-$ , obtained from independent analyses of the different  $W$ -intervals, are consistent within the uncertainties. The values of the  $A_{1/2}$  electrocoupling of the  $\Delta(1620)1/2^-$  state from the fit of the  $W$ -interval from

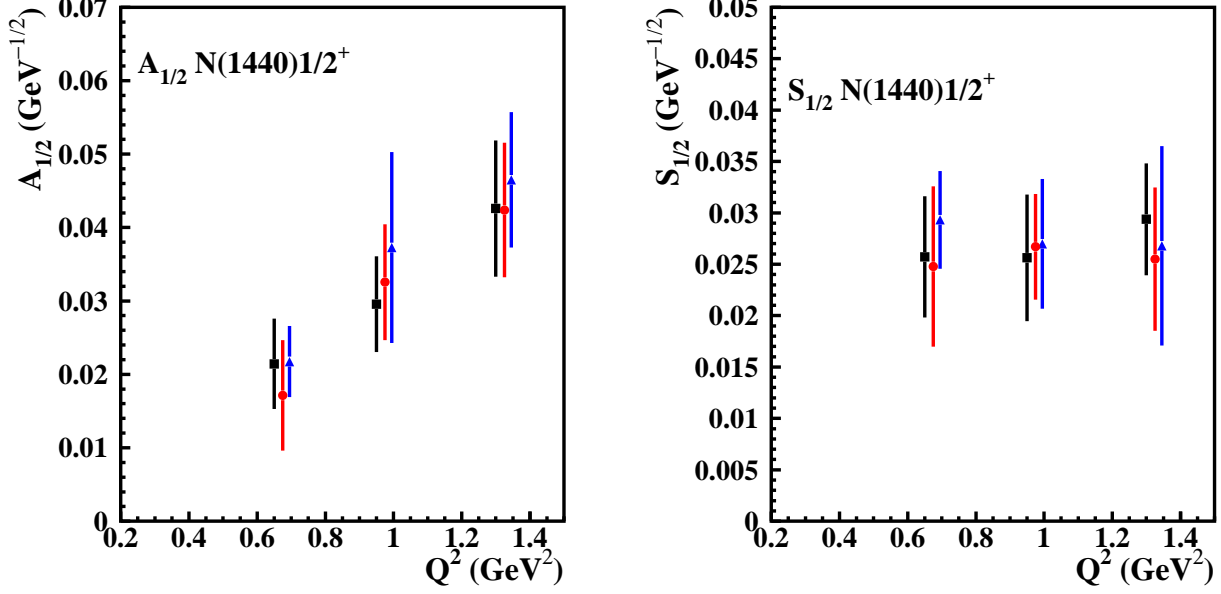


FIG. 8: (Color Online) Electrocouplings of the  $N(1440)1/2^+$  resonance determined from analysis of the CLAS  $\pi^+\pi^-p$  electroproduction data [24] carried out independently in three intervals of  $W$ :  $1.41 \text{ GeV} < W < 1.51 \text{ GeV}$  (black squares),  $1.46 \text{ GeV} < W < 1.56 \text{ GeV}$  (red circles), and  $1.51 \text{ GeV} < W < 1.61 \text{ GeV}$  (blue triangles).

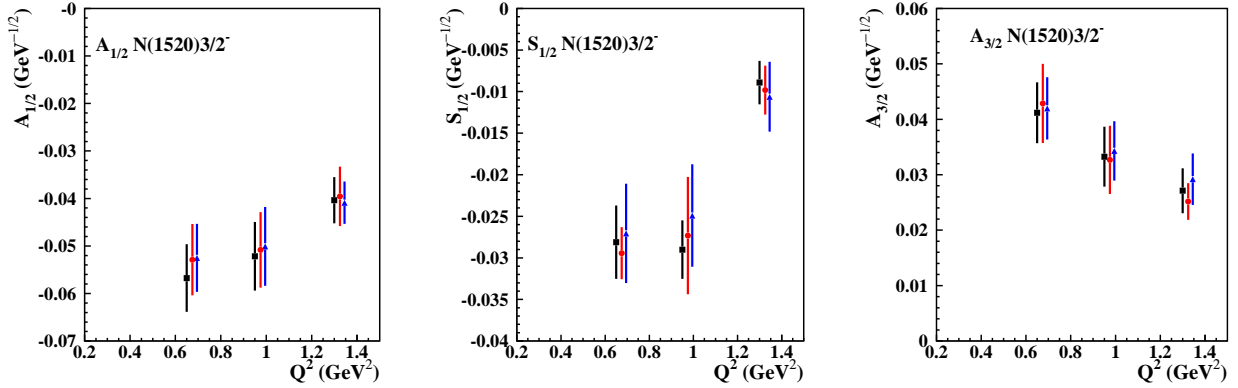


FIG. 9: (Color Online) Electrocouplings of the  $N(1520)3/2^-$  resonance determined from analysis of the CLAS  $\pi^+\pi^-p$  electroproduction data [24] carried out independently in three intervals of  $W$ :  $1.41 \text{ GeV} < W < 1.51 \text{ GeV}$  (black squares),  $1.46 \text{ GeV} < W < 1.56 \text{ GeV}$  (red circles), and  $1.51 \text{ GeV} < W < 1.61 \text{ GeV}$  (blue triangles).

1.51 GeV to 1.61 GeV are different in comparison to the fit results of the two others  $W$ -intervals. We consider the values of the  $\Delta(1620)1/2^-$  electrocouplings determined in the  $W$ -interval from 1.56 GeV to 1.66 GeV as the most reliable, since the others  $W$ -intervals overlap only over part of the resonance line width of the  $\Delta(1620)1/2^-$ . The consistent results on the  $\gamma_v p N^*$  electrocouplings from the independent analyses of different  $W$ -intervals strongly support the reliable extraction of these fundamental quantities, as well as the capability of the JM model to provide reliable information on the

$\gamma_v p N^*$  resonance electrocouplings from analysis of the data on exclusive charged double-pion electroproduction.

The final results on the  $N(1440)1/2^+$ ,  $N(1520)3/2^-$ , and  $\Delta(1620)1/2^-$  electrocouplings are listed in Tables VIII, IX, and X. They were determined from the fit of the CLAS data [24] in the  $W$ -intervals given in the captions of Tables VIII, IX, and X covering the three  $Q^2$ -bins centered at  $0.65 \text{ GeV}^2$ ,  $0.95 \text{ GeV}^2$ , and  $1.30 \text{ GeV}^2$ . The intervals over  $W$  within which the resonance electrocouplings were extracted were determined by the requirement that the selected  $W$  intervals overlap the area of



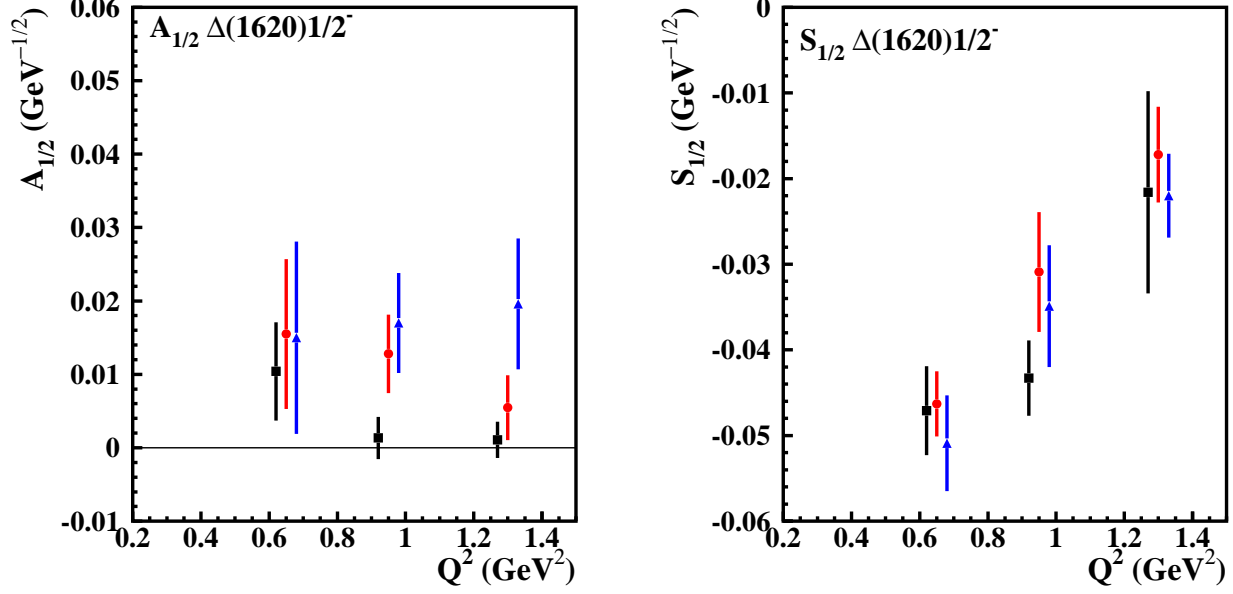


FIG. 10: (Color Online) Electrocouplings of the  $\Delta(1620)1/2^-$  resonance determined from analysis of the CLAS  $\pi^+\pi^-p$  electroproduction data [24] carried out independently in three intervals of  $W$ :  $1.51 \text{ GeV} < W < 1.61 \text{ GeV}$  (black squares),  $1.56 \text{ GeV} < W < 1.66 \text{ GeV}$  (red circles), and  $1.61 \text{ GeV} < W < 1.71 \text{ GeV}$  (blue triangles).

$Q^2$ , GeV <sup>2</sup>	$A_{1/2}$ , GeV <sup>-1/2</sup> *1000	$S_{1/2}$ GeV <sup>-1/2</sup> *1000
0.65	$21.4 \pm 6.2$	$25.7 \pm 5.9$
0.95	$29.6 \pm 6.5$	$25.6 \pm 6.2$
1.30	$42.6 \pm 9.3$	$29.4 \pm 5.5$

TABLE VIII: Electrocouplings of the  $N(1440)1/2^+$  resonance determined from this analysis of  $\pi^+\pi^-p$  electroproduction off the proton [24] at  $1.41 \text{ GeV} < W < 1.51 \text{ GeV}$  within the framework of the updated JM model described in Section II B.

$Q^2$ , GeV <sup>2</sup>	$A_{1/2}$ , GeV <sup>-1/2</sup> *1000	$S_{1/2}$ GeV <sup>-1/2</sup> *1000
0.65	$15.5 \pm 10.2$	$-46.3 \pm 3.8$
0.95	$12.5 \pm 5.4$	$-30.9 \pm 7.0$
1.30	$5.5 \pm 4.4$	$-17.2 \pm 5.6$

TABLE X: Electrocouplings of the  $\Delta(1620)1/2^-$  resonance determined from this analysis of  $\pi^+\pi^-p$  electroproduction off the proton [24] at  $1.56 \text{ GeV} < W < 1.66 \text{ GeV}$  within the framework of the updated JM model described in Section II B.

$Q^2$ , GeV <sup>2</sup>	$A_{1/2}$ , GeV <sup>-1/2</sup> *1000	$S_{1/2}$ , GeV <sup>-1/2</sup> *1000	$A_{3/2}$ , GeV <sup>-1/2</sup> *1000
0.65	$-52.9 \pm 7.5$	$-29.4 \pm 3.1$	$42.9 \pm 7.1$
0.95	$-50.8 \pm 7.9$	$-27.3 \pm 7.1$	$32.7 \pm 6.2$
1.30	$-39.6 \pm 6.3$	$-9.8 \pm 2.9$	$25.2 \pm 3.3$

TABLE IX: Electrocouplings of the  $N(1520)3/2^-$  resonance determined from this analysis of  $\pi^+\pi^-p$  electroproduction off the proton [24] at  $1.46 \text{ GeV} < W < 1.56 \text{ GeV}$  within the framework of the updated JM model described in Section II B.

masses below and above the central resonance mass values. The resonance electrocoupling uncertainties reflect both the experimental data uncertainties and the systematic uncertainties imposed by the extraction model.

The  $A_{1/2}$  electrocouplings of the  $N(1440)1/2^+$  state are positive and increase with  $Q^2$ , supporting the zero crossing observed for this electroexcitation amplitude

in our previous analyses of the CLAS  $N\pi$  and  $N\pi\pi$  electroproduction data [25, 27]. The  $A_{1/2}$  electrocouplings of the  $N(1520)3/2^-$  state are negative and increase with photon virtualities, confirming the local minimum at  $Q^2 \approx 0.45 \text{ GeV}^2$  observed in our previous analyses [25, 27]. The electroexcitation of the  $\Delta(1620)1/2^-$  resonance is dominated by longitudinal electrocouplings in the entire area of photon virtualities covered in our analysis,  $0.5 \text{ GeV}^2 < Q^2 < 1.5 \text{ GeV}^2$ .

In this analysis we also obtained the hadronic decay widths of the  $N(1440)1/2^+$ ,  $N(1520)3/2^-$ , and  $\Delta(1620)1/2^-$  resonances to the  $\pi\Delta$  and  $\rho p$  final states. These parameters were determined from the  $\pi^+\pi^-p$  electroproduction data [24] under simultaneous variations of the resonance masses,  $\gamma_v p N^*$  electrocouplings, and hadronic decay widths to the  $\pi\Delta$  and  $\rho N$  final states under the requirement of  $Q^2$ -independence of the resonance masses and hadronic decay parameters.

The  $N(1440)1/2^+$  and  $N(1520)3/2^-$  masses, as well as

Parameter	Current analysis of the CLAS $\pi^+\pi^-p$ data [24] at $0.5 \text{ GeV}^2 < Q^2 < 1.5 \text{ GeV}^2$	Previous analysis [27] of the CLAS $\pi^+\pi^-p$ data [23] 0.25 at $0.25 \text{ GeV}^2 < Q^2 < 0.6 \text{ GeV}^2$	RPP
Breit-Wigner mass, MeV	$1454 \pm 11$	$1458 \pm 12$	1420-1470 ( $\approx 1440$ )
Breit-Wigner width, MeV	$352 \pm 37$	$363 \pm 39$	200-450 ( $\approx 300$ )
$\pi\Delta$ partial decay width, MeV	$120 \pm 41$	$142 \pm 48$	
$\pi\Delta$ BF,	20%-52%	23%-58%	20%-30%
$\rho p$ partial decay width, MeV	$4.9 \pm 2.2$	$6.2 \pm 4.1$	
$\rho p$ BF	$< 2.0\%$	$< 2.0\%$	$< 8.0\%$

TABLE XI: Hadronic parameters of the  $N(1440)1/2^+$  resonance determined from the CLAS data [24] on  $\pi^+\pi^-p$  electroproduction off the proton within the framework of the updated JM model described in Section II B in comparison with the results of our previous analysis [27] and RPP [68].

Parameter	Current analysis of the CLAS $\pi^+\pi^-p$ data [24] at $0.5 \text{ GeV}^2 < Q^2 < 1.5 \text{ GeV}^2$	Previous analysis [24] of the CLAS $\pi^+\pi^-p$ data at $0.25 \text{ GeV}^2 < Q^2 < 0.6 \text{ GeV}^2$	RPP
Breit-Wigner mass, MeV	$1522 \pm 5$	$1521 \pm 4$	1515-1525 ( $\approx 1520$ )
Breit-Wigner width, MeV	$125 \pm 4$	$127 \pm 4$	100-125 ( $\approx 115$ )
$\pi\Delta$ partial decay width, MeV	$36 \pm 5$	$35 \pm 4$	
$\pi\Delta$ BF	25%-34%	24%-32%	15%-25%
$\rho p$ partial decay width, MeV	$13 \pm 6$	$16 \pm 5$	
$\rho p$ BF	4.8%-16%	8.4%-17%	15%-25%

TABLE XII: Hadronic parameters of the  $N(1520)3/2^-$  resonance determined from the CLAS data [24] on  $\pi^+\pi^-p$  electroproduction off the proton within the framework of the updated JM model described in Section II B in comparison with the results of our previous analysis [27] and RPP [68].

the branching fractions for the decays to the  $\pi\Delta$  and  $\rho N$  final states extracted in the fit of the data [24], are given in Tables XI and XII in comparison with the results of our previous analysis [27] of the CLAS  $\pi^+\pi^-p$  electroproduction data [23] carried out at smaller  $W$  and  $Q^2$ . The results of our current analysis on the  $N(1440)1/2^+$  and  $N(1520)3/2^-$  masses, and their total and partial hadronic decay widths to the  $\pi\Delta$  and  $\rho p$  final states are consistent. A successful description of the CLAS  $\pi^+\pi^-p$  electroproduction data over different and wide ranges of photon virtualities,  $0.25 \text{ GeV}^2 < Q^2 < 0.6 \text{ GeV}^2$  (previous analysis [27])  $0.5 \text{ GeV}^2 < Q^2 < 1.5 \text{ GeV}^2$  (current analysis), strongly support the reliable separation of the resonant and non-resonant contributions achieved within the framework of the JM model and the credible extraction of the  $N(1440)1/2^+$  and  $N(1520)3/2^-$  resonance parameters. Both the current and previous analyses of the CLAS  $\pi^+\pi^-p$  electroproduction data suggest that the  $\rho p$  hadronic decay widths of the  $N(1440)1/2^+$  and  $N(1520)3/2^-$  resonances are smaller than those reported in the RPP, and that the  $\pi\Delta$  hadronic decay widths of the  $N(1520)3/2^-$  are larger than those reported in RPP [68]. The successful description of the CLAS  $\pi^+\pi^-p$  electroproduction data [23, 24] in a wide area of  $Q^2$  from  $0.25 \text{ GeV}^2$  to  $1.5 \text{ GeV}^2$  achieved with  $Q^2$ -independent resonance hadronic parameters, makes the results presented in Tables XI and XII reliable. They offer new information on the hadronic decays of the  $N(1440)1/2^+$  and  $N(1520)3/2^-$  resonances to the  $\pi\Delta$  and  $\rho N$  final

states that may be considered as input for the upcoming RPP edition.

For the first time the hadronic decay parameters of the  $\Delta(1620)1/2^-$  resonance listed in Table XIII, have become available from the analysis of the  $\pi^+\pi^-p$  electroproduction data. The mass, total width, and the branching fractions for decays of the  $\Delta(1620)1/2^-$  to the  $\pi\Delta$  final states obtained in our analysis are in good agreement with the RPP results [68]. The current analysis suggests much larger values of the branching fractions for decays of the  $\Delta(1620)1/2^-$  to the  $\rho p$  final states in comparison with those presented in RPP. A successful description of the CLAS  $\pi^+\pi^-p$  electroproduction data [24] with  $Q^2$  independent values of the  $\Delta(1620)1/2^-$  hadronic decay widths strongly supports the branching fraction values listed in Table XIII. The large values determined for the branching fraction for decays of the  $\Delta(1620)1/2^-$  to the  $\rho p$  final states represent an interesting and unexpected result, since the  $\Delta(1620)1/2^-$  state is located in the sub-threshold area for  $\rho p$  electroproduction off the proton. The absence of  $\rho$  peaks in the data on the  $\pi^+\pi^-$  invariant mass distributions at  $W \approx 1.6 \text{ GeV}$ , in combination with large  $\rho p$  hadronic decays of the  $\Delta(1620)1/2^-$ , impose restrictions on the upper limits of the  $A_{1/2}$  electrocouplings for the  $\Delta(1620)1/2^-$  state, making their absolute values much smaller than those of the  $S_{1/2}$  electrocouplings.

Parameter	Current analysis of the CLAS $\pi^+\pi^-p$ data [24] at $0.5 \text{ GeV}^2 < Q^2 < 1.5 \text{ GeV}^2$	RPP
Breit-Wigner mass, MeV	$1631 \pm 12$	1600-1660 ( $\approx 1630$ )
Breit-Wigner width, MeV	$148 \pm 10$	130-150 ( $\approx 140$ )
$\pi\Delta$ partial decay width, MeV	$66 \pm 23$	
$\pi\Delta$ BF,	27%-64%	30%-60%
$\rho p$ partial decay width, MeV	$70 \pm 21$	
$\rho p$ BF	31%-63%	7%-25%

TABLE XIII: Hadronic parameters of the  $\Delta(1620)1/2^-$  resonance determined from the CLAS data [24] on  $\pi^+\pi^-p$  electroproduction off the proton within the framework of the updated JM model described in Section II B in comparison with RPP [68].

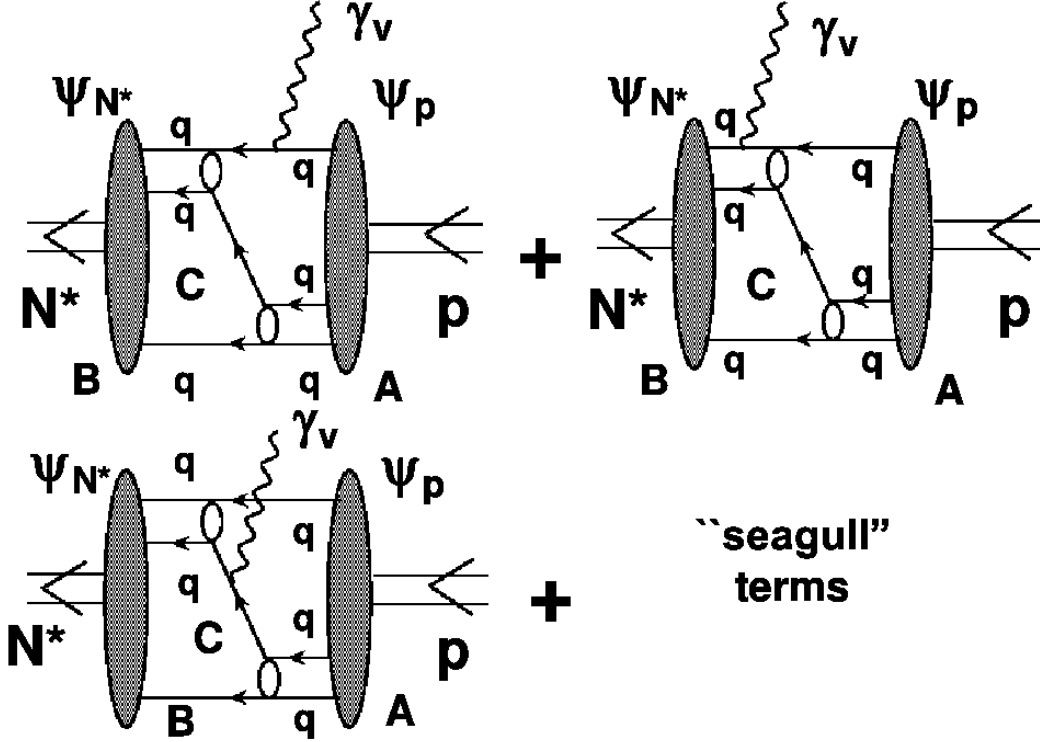


FIG. 11: Description of the resonance electroexcitation amplitudes within the framework of DSEQCD [3, 31, 33]: A) the amplitude for the transition  $p \rightarrow$  three dressed quarks or the ground state wave function  $\psi_p$ , B) the amplitude for the transition three dressed quarks  $\rightarrow N^*$  or the excited nucleon state wave function  $\psi_{N^*}$ , C) the amplitude that describes the interaction between the virtual photon and three dressed quarks bound by the non-perturbative strong interaction between pairs of correlated quarks (di-quark) and by the dressed quark exchange between the di-quark pair and third quark. The virtual photon interactions with the quark and di-quark currents are shown on the left and top right diagrams, respectively. The di-quark currents incorporate the transitions between di-quarks of the same and different quantum numbers. The full  $N \rightarrow N^*$  transition amplitude can be found in Fig. C1 of Ref. [31].

## V. IMPACT ON STUDIES OF THE $N^*$ STRUCTURE FROM THE NEW CLAS RESULTS

In this section we discuss the impact of the new CLAS results on the  $N(1440)1/2^+$ ,  $N(1520)3/2^-$ , and  $\Delta(1620)1/2^-$  electrocouplings and their partial hadronic decay widths to the  $\pi\Delta$  and  $\rho N$  final states on the con-

temporary understanding of the structure of these states. We will also outline new possibilities for hadron structure theory to employ these experimental results in order to explore how the dynamical properties of three constituent dressed quarks inside the resonance quark core emerge from QCD.

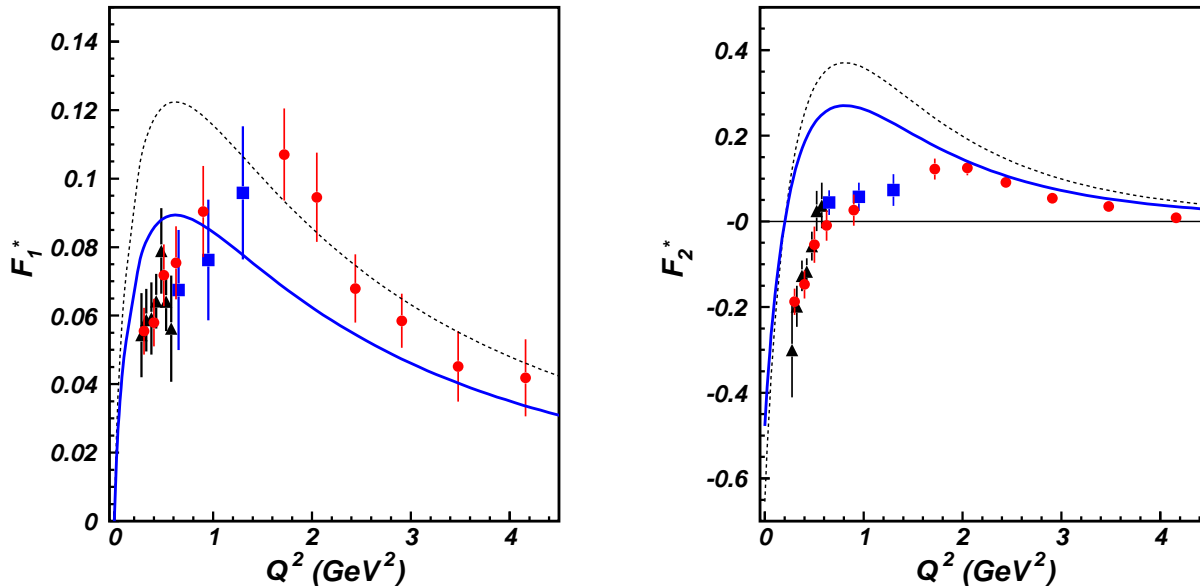


FIG. 12: (Color Online) The  $F_1^*$  and  $F_2^*$  transition  $p \rightarrow N(1440)1/2^+$  form factors: experimental results from analyses of the CLAS data on  $N\pi$  [25] (red circles) and  $\pi^+\pi^-p$  [27] (black triangles) electroproduction off the proton and the results of this present work (blue squares). The data are shown in comparison with DSEQCD evaluations [33] start from the QCD Lagrangian (black dashed line) and after accounting for the meson-baryon cloud contributions as described in Section V A (blue thick solid line).

### A. $N(1440)1/2^+$ and $N(1520)3/2^-$ Resonances

Previous studies of the  $N(1440)1/2^+$  and  $N(1520)3/2^-$  resonances with the CLAS detector [25, 27] have provided the dominant part of the world-wide information available on their electrocouplings in a wide range of photon virtualities  $0.25 \text{ GeV}^2 < Q^2 < 5.0 \text{ GeV}^2$ . This paper extends the CLAS results on the  $N(1440)1/2^+$  and  $N(1520)3/2^-$   $\gamma_v p N^*$  electrocouplings in the range of photon virtualities from  $0.5 \text{ GeV}^2$  to  $1.5 \text{ GeV}^2$  where there is limited availability of data. Previous studies of  $\pi^+\pi^-p$  electroproduction [27] have allowed us to determine the  $N(1440)1/2^+$  and  $N(1520)3/2^-$  partial decay widths to the  $\pi\Delta$  and  $\rho p$  final states. Our current studies confirmed the previous results [27] on these hadronic decays. Currently the  $N(1440)1/2^+$  and  $N(1520)3/2^-$  states, together with the  $\Delta(1232)3/2^+$  and  $N(1535)1/2^-$  resonances [1], represent the most explored excited nucleon states. Detailed information on the electrocouplings of these states that are available for the first time from CLAS, have already provided a profound impact on the contemporary understanding of the nucleon resonance structure [1, 2, 27].

Recent progress in the studies of resonance structure achieved within the framework of the Dyson-Schwinger Equations of QCD (DSEQCD) [3, 31, 33] has allowed us for the first time to interpret the experimental results on the nucleon elastic form factors, as well as the magnetic  $p \rightarrow \Delta$  and  $p \rightarrow N(1440)1/2^+$  Dirac ( $F_1^*$ ) and Pauli

( $F_2^*$ ) transition from factors start from the QCD Lagrangian. Currently this approach is capable of evaluating the contributions from the quark core of three dressed quarks to the nucleon elastic and  $p \rightarrow N^*$  transition form factors. DSEQCD approaches describe the ground and excited nucleons as bound systems of three dressed quarks that represent the complex objects generated non-perturbatively from an infinite number of QCD quarks and gauge gluons. The dynamical properties of dressed quarks, the momentum dependent mass  $M(p)$  and form factors, that enter into the quark electromagnetic current, are determined start from the QCD Lagrangian employing the towers of gap equations for quarks and gluons [3]. The ground and excited nucleon state masses and the transition amplitudes,  $p \rightarrow$  three dressed quarks (the ground state wave function) and three dressed quarks  $\rightarrow N^*$  (the excited nucleon state wave function), are obtained in a Poincaré covariant approach employing Faddeev equations for the three dressed quarks. The non-perturbative interactions between the three dressed quarks are reduced to a quark-quark interaction that generates pairs of correlated quarks, the so-called dynamical di-quark, and dressed quark exchanges between the di-quark pair and third quark shown in the parts labeled “C” in Fig. 11 [3, 70]. The ground and excited nucleon state masses emerge as poles in the energy dependence of the amplitude with the respective spin-parity that comes from the Faddeev equation solution. The ground/excited nucleon state wave functions represent

the residues of the Faddeev equation solutions at the respective pole positions. The resonance electroexcitation amplitudes, depicted in Fig. 11, are evaluated as the product of three amplitudes: A) ground state  $p \rightarrow$  three dressed quarks, B) three dressed quarks  $\rightarrow$  resonance  $N^*$ , and C) interaction between real/virtual photons and the three dressed quarks. The latter part C is described mostly by real/virtual photon couplings to the dressed quark and di-quark pair currents. All details on the evaluations of resonance electroexcitation amplitudes can be found in Refs. [31, 33].

The resonance electroexcitation amplitudes shown in Fig. 11 should be sensitive to the momentum dependence of the dressed quark mass  $M(p)$ , since it affects all quark propagators and dressed quark currents. Moreover, it was shown in Refs. [31, 33] that the momentum dependence of the dressed quark mass has a pronounced influence on the wave functions of the ground and excited nucleon states. DSEQCD studies of experimental results on elastic nucleon form factors [35] confirmed these expectations and revealed considerable sensitivity of the nucleon elastic form factors to the momentum dependence of the dressed quark mass function. It was found that the location of the zero crossing for the ratio  $\mu_p G_E/G_M(Q^2)$  is determined by the derivative of the dressed quark mass function  $M(p)$ .

The need to employ a momentum-dependent dressed quark mass function was conclusively demonstrated in the studies of the  $N \rightarrow \Delta$  magnetic transition form factor within the DSEQCD framework [3]. Computations employing a dressed quark with a momentum-independent mass generated by simplified contact quark-quark interactions were able to describe the experimental results only in a very limited range of photon virtualities  $Q^2 < 3.0 \text{ GeV}^2$ . Instead, the DSEQCD evaluation with running quark mass successfully reproduced the experimental data at  $Q^2 > 1.0 \text{ GeV}^2$  in the entire range of photon virtualities covered by measurements reaching up to  $8.0 \text{ GeV}^2$ .

The recent DSEQCD studies of the  $N(1440)1/2^+$  resonance electroexcitation [33] derive from a realistic quark-quark interaction that generates a momentum-dependent dressed quark mass function. The evaluated contributions from the quark core to the Dirac  $F_1^*$  and to the Pauli  $F_2^*$   $p \rightarrow N(1440)1/2^+$  transition form factors are shown in Fig. 12 by the dashed lines in comparison with the CLAS experimental results published in Refs. [25, 27], as well as with those obtained in this present work. DSEQCD reasonably reproduces the experimental results for  $Q^2 > 2.5 \text{ GeV}^2$ . However, a pronounced disagreement for  $Q^2 < 1.0 \text{ GeV}^2$ , in particular, for the Pauli  $F_2^*$  form factor, suggests significant contributions from degrees of freedom other than the quark core, presumably the meson-baryon cloud found in the global multi-channel analysis of exclusive meson photo-, electro-, and hadroproduction data [43]. These contributions are still beyond the scope of DSEQCD studies [33]. However, we have to account for the fraction of the meson-baryon

degrees of freedom in the wave functions of the ground and excited nucleon states. We choose to estimate this contribution by multiplying the  $p \rightarrow N(1440)1/2^+$  transition form factors computed within the DSEQCD approach [33] by a common  $Q^2$ -independent factor fit to the data for  $Q^2 > 3.0 \text{ GeV}^2$ , where the meson-baryon cloud contributions are much smaller than those from the quark core. The fit value of this factor of 0.73 is consistent with the results of a recent advanced light front quark model [45], which employs the parameterization of running quark mass function in spirit of DSEQCD [3]. The  $p \rightarrow N(1440)1/2^+$  transition form factors obtained in this way are shown in Fig. 12 by the solid blue lines. A good description of the experimental results for  $Q^2 > 1.5 \text{ GeV}^2$  is achieved within the entire range of photon virtualities covered by the measurements.

The dressed quark mass function used in the DSEQCD computations of the  $p \rightarrow N(1440)1/2^+$  transition form factors [33] is *exactly the same* as that employed in the previous evaluations of the nucleon elastic and magnetic  $p \rightarrow \Delta$  transition form factors [31, 35]. The  $\Delta(1232)3/2^+$  and  $N(1440)1/2^+$  excited nucleon states have a distinctively different structure: spin-flavor flip for the  $\Delta(1232)3/2^+$  and the first radial excitation of three dressed quarks for the  $N(1440)1/2^+$ . A successful description of the elastic and transition form factors to nucleon resonances of distinctively different structure achieved with the same dressed quark mass function strongly underlines:

- the relevance of dynamical dressed quarks with the properties predicted by the DSEQCD approach [3] as constituents of the quark cores for the structure of the ground and excited nucleon states;
- the capability of the DSEQCD approach [31, 33] to map out the dressed quark mass function from the experimental results on the  $Q^2$ -evolution of the nucleon elastic and  $p \rightarrow N^*$  transition form factors ( $\gamma_v p N^*$  electrocouplings) from a combined analysis.

Consistent results on the momentum dependence of the dressed quark mass function obtained from independent analyses of nucleon elastic and  $p \rightarrow N^*$  form factors, i.e.  $\gamma_v p N^*$  electrocouplings for the transition to excited nucleons with different quantum numbers, are critical in order to prove the reliable access to this fundamental quantity.

DSEQCD analyses [31, 33] of the CLAS results on the  $p \rightarrow \Delta$  and  $p \rightarrow N(1440)1/2^+$  transition form factors (the latter shown in Fig. 13) have demonstrated the capability of accessing the dressed quark mass function from the experimental data for the first time. Studies of the dressed quark mass function will address the most challenging and still open problems of the Standard Model on the nature of the dominant part of the hadron mass, quark-gluon confinement, its emergence from QCD, and its relation to dynamical chiral symme-

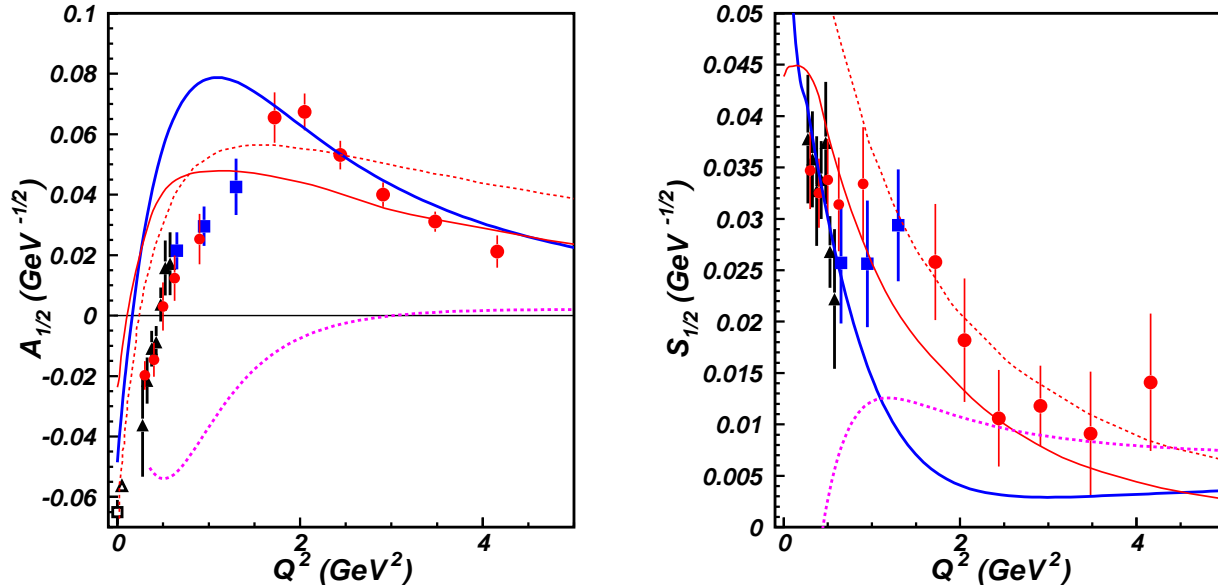


FIG. 13: (Color Online) The  $A_{1/2}$  and  $S_{1/2}$   $\gamma_v p N^*$  electrocouplings of the  $N(1440)1/2^+$  resonance: experimental results from analyses of the CLAS data on  $N\pi$  [25] (red circles) and  $\pi^+\pi^-p$  [27] (black triangles) electroproduction off the proton and the results of this work (blue squares). The data are shown in comparison with the DSEQCD evaluations [33] (blue thick solid) and the results from constituent quark models that account for the contributions from both the quark core and the meson-baryon cloud: [45] (thin red solid) and [46] (thin red dashed). The calculations of thin red line includes pion loops and a parametrization of the running quark mass, and the calculations of dashed red line contains  $N\sigma$  contributions and fixed quark mass. The meson-baryon cloud contributions obtained from the experimental data (see Section V A) are shown by the magenta thick dashed lines.

try breaking, which is expected to be the source of more than 98% of the hadron mass in universe [3].

Recent advances in the development of the constituent quark models make it possible to extend the  $Q^2$ -range for a better description of the  $\gamma_v p N^*$  electrocouplings in comparison with DSEQCD approaches, taking into account both contributions from the quark core and the meson-baryon cloud. The two models [45, 46] describe the structure of the  $N(1440)1/2^+$  resonance as an interplay between the contributions from the inner core of three dressed quarks in the first radial excitation and an external meson-baryon cloud. Both approaches treat the quark core contributions within the light front framework. The first model [45] employs a phenomenological momentum-dependent dressed quark mass motivated by the DSEQCD results [31, 33], while the second [46] employs constituent quarks of momentum-independent mass. The meson baryon cloud is modeled by  $\pi N$  loops in the first approach [45], while the  $\sigma p$  loops are employed in the second approach [46]. The CLAS experimental results on the  $A_{1/2}$  and  $S_{1/2}$   $\gamma_v p N^*$  electrocouplings of the  $N(1440)1/2^+$  resonance are shown in Fig. 13 in comparison with the expectations from DSEQCD [33] and from the aforementioned two advanced constituent quark models [45, 46]. Accounting for the meson-baryon cloud contributions allowed us to considerably improve the descrip-

tion of the experimental data at  $Q^2 < 2.0 \text{ GeV}^2$ , confirming the relevance of meson-baryon degrees of freedom in the  $N(1440)1/2^+$  structure at these distances that had previously been established in multi-channel analyses of exclusive meson photo-, electro-, and hadroproduction experimental data [43].

The CLAS results on the  $\gamma_v p N^*$  electrocouplings of the  $N(1520)3/2^-$  resonance are shown in Fig. 14. The currently available models for the description of the structure of this state account for quark core contributions only. The quark core contributions to the  $\gamma_v p N^*$  electrocouplings of most well-established excited nucleon states were explored within the framework of two conceptually different approaches: a) hypercentral constituent quark model [49] and b) Bethe-Salpeter approach that employs structureless constituent quarks with momentum-independent mass and an instanton quark-quark interaction [37]. The hypercentral constituent quark model provides a reasonable description of the experimental results at  $Q^2 > 1.0 \text{ GeV}^2$  as shown in Fig. 14. At smaller photon virtualities there are substantial discrepancies between the model [49] and the CLAS results. A similar observation comes from the comparison of the CLAS results with the Bethe-Salpeter approach [37]. Estimates for the contributions from the meson-baryon cloud to the structure of the  $N(1520)3/2^-$  resonance were ob-

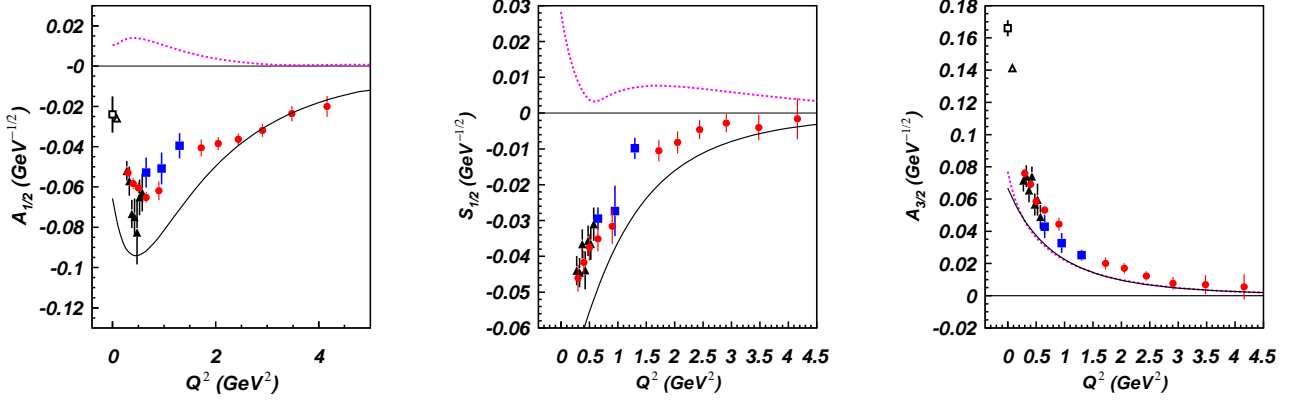


FIG. 14: (Color Online) The  $A_{1/2}$ ,  $S_{1/2}$ , and  $A_{3/2}$   $\gamma_v p N^*$  electrocouplings of the  $N(1520)3/2^-$  resonance: experimental results from analyses of the CLAS data on  $N\pi$  [25] (red circles) and  $\pi^+\pi^-p$  [27] (black triangles) electroproduction off the proton and the results of this present work (blue squares). The data are shown in comparison with the predictions of the hypercentral quark model [49] (thin black solid). The meson-baryon cloud contributions obtained in a global multi-channel  $N\pi$  photo-, electro-, and hadroproduction data analysis [43] are shown by the thick dashed magenta lines.

tained in Ref. [43] from a global multi-channel analysis of the experimental data on exclusive pion photo-, electro-, and hadroproduction. The absolute values of the meson-baryon cloud shown in Fig. 14 are maximal at small photon virtualities where discrepancies between the quark model expectations and the experimental data are largest. Hence, the meson-baryon cloud contributions may explain the difference between the CLAS data and the quark model expectations for the  $\gamma_v p N^*$  electrocouplings of the  $N(1520)3/2^-$  resonance. The aforementioned studies of the CLAS data in Fig. 14 suggest that the structure of the  $N(1520)3/2^-$  resonance arises from the contributions from the inner core of three dressed quarks in the first orbital excitation with  $L = 1$  and the external meson-baryon cloud. The contributions from the meson-baryon cloud are strongly dependent on the helicity of the  $N^*$  electroexcitation amplitudes. They decrease with photon virtuality  $Q^2$ .

The CLAS data on the  $\gamma_v p N^*$  electrocouplings of the  $N(1440)1/2^+$  and  $N(1520)3/2^-$  resonances, together with the results from previous studies [25] and recent analyses of the  $N^*$  electroexcitations in the third resonance region [15, 71], strongly suggest that the structure of nucleon resonances for  $Q^2 < 5.0 \text{ GeV}^2$  is determined by a complex interplay between the inner core of three dressed quarks bound to the states with the quantum numbers of the nucleon resonance and the external meson-baryon cloud. The quark core fully determines the spins and parities of the resonances, while the meson-baryon cloud affects the resonance masses, electroexcitation amplitudes, and hadronic decay widths.

Access to the different components in the resonance structure represents a challenging objective. The credible DSEQCD evaluation of the quark core contributions to the electrocouplings of the  $N(1440)1/2^+$  [33] allows us

to estimate the meson-baryon cloud contributions as the difference between the fit of the experimental results and the quark core electroexcitation amplitudes from DSE-QCD [33]. The meson-baryon cloud contributions to the electrocouplings of the  $N(1440)1/2^+$  state obtained in this way are shown in Fig. 13 by the thick dashed magenta lines. The meson-baryon cloud contributions to the  $A_{1/2}$  electrocouplings of the  $N(1440)1/2^+$  are maximal for  $Q^2 < 1.0 \text{ GeV}^2$ . At  $Q^2 > 1.0 \text{ GeV}^2$  they rapidly decrease with photon virtualities and become negligible for  $Q^2 > 2.0 \text{ GeV}^2$ . The meson-baryon cloud contributions to the  $S_{1/2}$  electrocouplings of the  $N(1440)1/2^+$  show a rather slow  $Q^2$ -evolution for  $2.0 \text{ GeV}^2 < Q^2 < 5.0 \text{ GeV}^2$ . The  $S_{1/2}$  electrocouplings of the  $N(1440)1/2^+$  are proportional to the difference

$$S_{1/2} \sim F_1^* - \frac{Q^2}{(M_R - M_N)^2} F_2^*, \quad (3)$$

where  $M_R$  and  $M_N$  are the  $N(1440)1/2^+$  and nucleon masses, respectively. For  $Q^2 > 2.0 \text{ GeV}^2$ , the contributions from the quark core almost cancel out, making the  $S_{1/2}$  electrocouplings of the  $N(1440)1/2^+$  more sensitive to the meson-baryon cloud contributions for  $Q^2 > 2.0 \text{ GeV}^2$ .

The analysis of the CLAS data has revealed a substantial dependence of the meson-baryon cloud contributions on the quantum numbers of the excited nucleon states and the transition helicity amplitudes. The magnitudes of the meson-baryon dressing amplitudes for the  $A_{1/2}$  electrocouplings of the  $N(1520)3/2^-$  are much smaller than for either the  $S_{1/2}$  or  $A_{3/2}$  electrocouplings (see Fig. 14), as well as with the  $A_{1/2}$  electrocoupling for the  $N(1440)1/2^+$  (see Fig. 13). This makes the  $A_{1/2}$  electrocoupling of the  $N(1520)3/2^-$  attractive for the studies of quark degrees of freedom in the structure of the

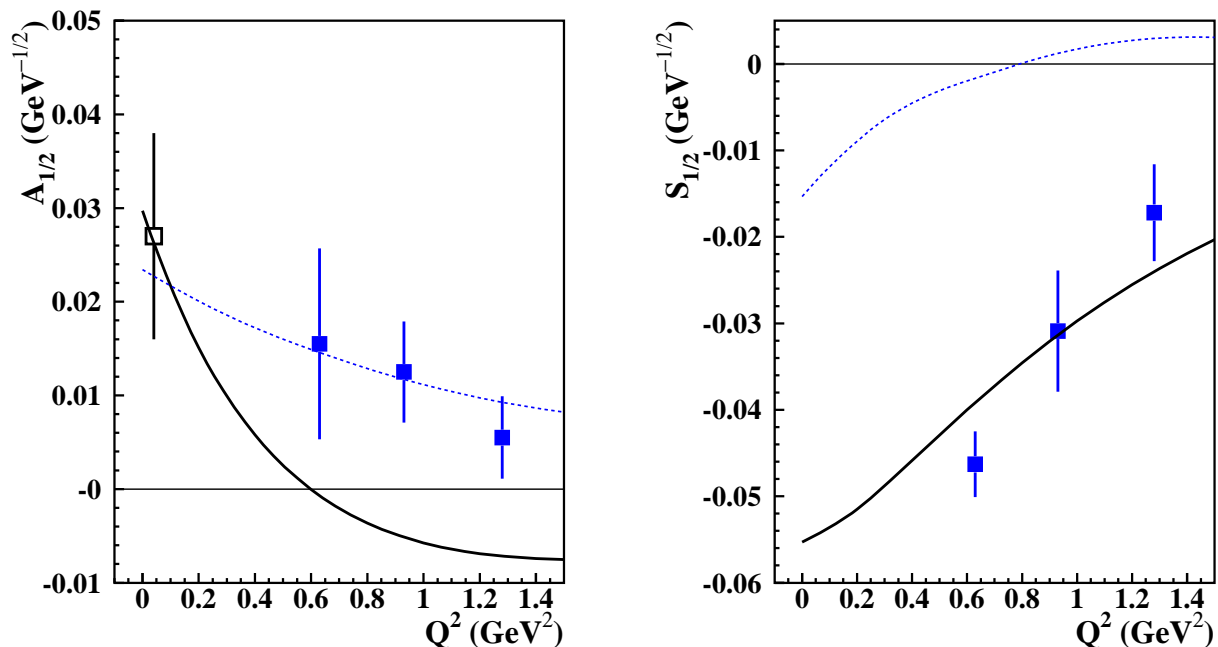


FIG. 15: (Color Online) The first results on the  $A_{1/2}$  and  $S_{1/2}$   $\gamma_v p N^*$  electrocouplings of the  $\Delta(1620)1/2^-$  resonance from the CLAS data on  $\pi^+\pi^-p$  electroproduction off the proton [24] in comparison with a hypercentral constituent quark model [49] (thick black solid lines) and the Bethe-Salpeter approach [37] (blue dashed lines). The photocoupling value is taken from the RPP [68].

$N(1520)3/2^-$  resonance.

Studies of the parton content of excited nucleons have been already initiated by the Regensburg University theory group [28, 30]. Recent developments in the Light-Cone-Sum-Rule (LCSR) approach allowed us for the first time to determine the partonic structure of the  $N(1535)1/2^-$  resonance [29] from the CLAS experimental results on the electrocouplings of this state for  $Q^2 > 2.0 \text{ GeV}^2$  [25]. The analysis of the  $N(1520)3/2^-$  electrocouplings within the framework of the LCSR approach were carried out in Ref. [72]. However, this approach employs quark distribution amplitudes for the nucleon ground states only. Future LCSR evaluations of the  $p \rightarrow N(1520)3/2^-$  electromagnetic transition amplitudes that incorporate the  $N(1520)3/2^-$  quark distribution amplitudes are needed in order to explore the partonic structure of the  $N(1520)3/2^-$  resonance.

### B. $\Delta(1620)1/2^-$ Resonance

The  $\gamma_v p N^*$  electrocouplings and the partial  $\pi\Delta$  and  $\rho p$  hadronic decay widths (see Table XIII) of the  $\Delta(1620)1/2^-$  resonance obtained for the first time from CLAS data on  $\pi^+\pi^-p$  electroproduction off the proton [24] have revealed very unusual properties of this state (Fig. 15). Currently it is the only well-established  $N^*$  state produced via electroexcitation that is dominated by the longitudinal  $S_{1/2}$  amplitude for  $0.5 \text{ GeV}^2 < Q^2 < 1.5 \text{ GeV}^2$ . The  $\rho p$  channel opens for the central

$\rho$  mass at the threshold of  $W=1.71 \text{ GeV}$ . Despite of the much smaller central mass  $1.62 \text{ GeV}$ , the  $\Delta(1620)1/2^+$  state has a large branching fraction for decays to the  $\rho p$  final state as listed in Table XIII.

The attempts to describe the electrocouplings of the  $\Delta(1620)1/2^-$  resonance within the framework of the constituent quark models, accounting for the contributions from only three dressed quarks in the first orbital excitation that belongs to the  $[70,1^-]$   $SU(6)$  spin-flavor multiplet, were not successful. As shown in Fig 15, the hypercentral constituent quark model [49] does allow for a reasonable description of the longitudinal electrocouplings, but it underestimates the transverse  $A_{1/2}$  electrocouplings. Instead, the above-mentioned Bethe-Salpeter approach [37] offers a good description of the transverse  $A_{1/2}$  electrocoupling of the  $\Delta(1620)1/2^-$ , but underestimates the longitudinal  $S_{1/2}$  electrocouplings. The unquenched constituent quark models [73] currently employed in the studies of mesons offer a promising opportunity to explore both the hadron wave functions and the hadronic decays. The extension of these approaches into the baryon sector looks promising in order to understand the nature of the  $\Delta(1620)1/2^-$  resonance from the combined analysis of the electroexcitation amplitudes and the hadronic decays of this resonance.

The large branching fraction for the hadronic decays to the  $\rho p$  final state of the deeply sub-threshold  $\Delta(1620)1/2^-$  state makes it attractive to search for an admixture of exotic configurations such as  $qqq(q\bar{q})$  that may facilitate the resonance decays to the  $\rho p$  final state.



## VI. SUMMARY AND OUTLOOK

Phenomenological analysis of CLAS data [24] on  $\pi^+\pi^-p$  electroproduction off the proton at invariant masses of the final hadron system  $1.40 \text{ GeV} < W < 1.82 \text{ GeV}$  and photon virtualities  $Q^2$  from  $0.5 \text{ GeV}^2$  to  $1.5 \text{ GeV}^2$  was carried out with the primary objective of determining the  $\gamma_v p N^*$  resonance electrocouplings and their partial hadronic decay widths to the  $\pi\Delta$  and  $\rho p$  final states for all prominent  $N^*$  states with masses below  $1.64 \text{ GeV}$ . The JM reaction model [26, 27] previously employed for the extraction of the resonance parameters from  $\pi^+\pi^-p$  electroproduction data [23] was further developed for extraction of the resonance parameters in a wider area of  $W$  and  $Q^2$ . In order to describe the data [24] on the final hadron distributions over the  $\alpha_i$  angles for  $W > 1.5 \text{ GeV}$ , the phases of the direct double-pion electroproduction amplitudes were implemented and fit to the measured nine one-fold differential cross sections. The updated JM model provides a good description of all available CLAS data on  $\pi^+\pi^-p$  electroproduction off the proton at  $1.40 \text{ GeV} < W < 1.82 \text{ GeV}$  and  $Q^2$  from  $0.5 \text{ GeV}^2$  to  $1.5 \text{ GeV}^2$ . The achieved quality of the data fit [24] is comparable to that obtained in reaction models employed previously for extraction of the resonance electrocouplings from CLAS data on  $N\pi$  [15, 25] and  $\pi^+\pi^-p$  [27] electroproduction off the proton. The contributions to charged double-pion electroproduction off the proton from all relevant meson-baryon channels and direct double pion production mechanisms determined from CLAS data within the framework of the updated JM model, shown in Fig. 5, are of interest for the future modeling of different exclusive meson electroproduction channels that are relevant in the resonance region. These results can also be used in global multi-channel analyses aimed at extraction of the resonance parameters from all available data on exclusive meson photo-, electro-, and hadroproduction.

The  $\gamma_v p N^*$  electrocouplings of the  $N(1440)1/2^+$  and  $N(1520)3/2^-$  resonances were determined from the exclusive charged double-pion electroproduction cross sections measured with CLAS at  $Q^2$  from  $0.5 \text{ GeV}^2$  to  $1.5 \text{ GeV}^2$ . Consistent values of the  $N(1440)1/2^+$  and  $N(1520)3/2^-$  electrocouplings obtained in independent analyses of three  $W$ -intervals, where the non-resonant contributions are different, strongly support the reliable extraction of these fundamental quantities. Furthermore, the hadronic decay widths of these resonances to the  $\pi\Delta$  and  $\rho p$  final states obtained in our analysis are consistent with those previously determined in this exclusive channel at smaller photon virtualities  $Q^2 < 0.55 \text{ GeV}^2$  [27]. Successful description of the CLAS  $\pi^+\pi^-p$  electroproduction data [23, 24] in a wide range of photon virtualities from  $0.25 \text{ GeV}^2$  to  $1.5 \text{ GeV}^2$  with  $Q^2$ -independent hadronic decay widths of the contributing resonances, supports a reliable separation between the resonant and non-resonant contributions achieved in the updated JM model and confirm reliable extraction of the resonance

parameters. The  $\Delta(1620)1/2^-$  resonance decays preferentially to the  $N\pi\pi$  final state. The  $\pi^+\pi^-p$  exclusive electroproduction off the proton represents the major source of information on the electrocouplings of this resonance. Our studies provide for the first time information on the  $\gamma_v p N^*$  electrocouplings and the  $\pi\Delta$  and  $\rho p$  partial hadronic decay widths of the  $\Delta(1620)1/2^-$  resonance.

Due to the recent progress in DSEQCD studies of excited nucleon states [3, 31], the first evaluations of the  $p \rightarrow N(1440)1/2^+$  Dirac  $F_1^*$  and Pauli  $F_2^*$  transition form factors starting from the QCD Lagrangian have recently become available [33]. A good description of the CLAS experimental results was obtained at  $Q^2 > 2.0 \text{ GeV}^2$  in the DSEQCD approach. In this application the same momentum-dependent dressed quark mass function was employed that was also used in the previous DSEQCD computations of the nucleon elastic [35] and magnetic  $p \rightarrow \Delta$  transition form factors [31]. A successful description of the nucleon elastic and electromagnetic transition form factors to excited nucleon states of distinctly different structure strongly supports a reliable access to the dressed quark mass function achieved in the analysis [33]. Mapping out the dressed quark mass function from available and future data on  $p \rightarrow N^*$  transition form factors will address the most challenging and still open problems of the Standard Model on the nature of the dominant part of the hadron mass, quark-gluon confinement, and their emergence from QCD [2, 3]. These prospects motivate the future studies of the excited nucleon state structure at high photon virtualities from  $5 \text{ GeV}^2$  to  $12 \text{ GeV}^2$  with the CLAS12 detector after the completion of the Jefferson Lab 12 GeV upgrade [2, 74, 75, 77].

Analyses of the experimental results on the  $\gamma_v p N^*$  electrocouplings of the  $N(1440)1/2^+$ ,  $N(1520)3/2^-$ , and  $\Delta(1620)1/2^-$  resonances in the entire range of photon virtualities covered by the measurements employing the DSEQCD approach [31, 33], advanced quark models [37, 45, 46], and a global multi-channel analysis [41–43], have convincingly demonstrated that their structure at  $Q^2 < 5.0 \text{ GeV}^2$  is determined by a complex interplay between the inner core of three dressed quarks and the external meson-baryon cloud. A successful description of the quark core contributions to the electrocouplings of the  $N(1440)1/2^+$  resonance within the framework of DSEQCD [33] makes it possible to outline meson-baryon cloud contributions for this state at the resonant point ( $W = M_{N^*}$ ) from the experimental results on the  $\gamma_v p N^*$  electrocouplings. We observed pronounced differences for the meson-baryon cloud contributions to different electroexcitation amplitudes and their strong dependence on the quantum numbers of the excited nucleon state and photon virtuality. In particular, small contributions from the meson-baryon cloud to the  $A_{1/2}$  electrocouplings of the  $N(1520)3/2^-$  make this resonance attractive for the exploration of its quark components. The studies of resonance electrocouplings over the full spectrum of excited nucleon states of different quantum numbers are critical in order to explore different components in the  $N^*$  struc-

ture.

Available for the first time,  $\Delta(1620)1/2^-$  resonance electrocouplings and hadronic decay widths to the  $\pi\Delta$  and  $\rho p$  final states have demonstrated a rather peculiar behavior. The  $\Delta(1620)1/2^-$  state is the only known resonance produced via electroexcitation that is dominated by the longitudinal  $S_{1/2}$  electrocoupling in a wide range of photon virtualities  $0.5 \text{ GeV}^2 < Q^2 < 1.5 \text{ GeV}^2$ . Furthermore, the  $\Delta(1620)1/2^-$  resonance has a large branching fraction (above 30%) for the decay into the  $\rho N$  final states. This is a rather unusual feature for decays of a resonance located in the deeply sub-threshold region for the production of the  $\rho p$  final state. Failures in describing the  $\Delta(1620)1/2^-$  electrocouplings within the framework of quark models that account for the contributions of the quark core only [37, 49], indicate that the structure of this state can be more complex than that assumed in quark models described by the orbital excitation of three quarks with the total orbital momentum  $L = 1$ . Further experimental data are needed in order to establish the nature of this state. In the near term future, new CLAS results on the  $\Delta(1620)1/2^-$  electrocouplings are expected at photon virtualities from  $0.3 \text{ GeV}^2$  to  $1.0 \text{ GeV}^2$  with a much finer  $Q^2$ -binning [76]. The results on the  $\Delta(1620)1/2^-$  electrocouplings from CLAS data on charged double-pion electroproduction off the proton eventually will also be extended in  $Q^2$  up to  $5.0 \text{ GeV}^2$ . Further developments in hadron structure theory that will allow us to perform a combined analysis of the resonance electrocouplings and

hadronic decay widths are critical in order to understand the nature of the  $\Delta(1620)1/2^-$  state. A search for contributions from exotic  $qqq(q\bar{q})$  configurations to the structure of this state that may facilitate the decays of the  $\Delta(1620)1/2^-$  resonance to the  $\rho p$  final state are of particular interest.

## VII. ACKNOWLEDGMENTS

We would like to acknowledge the outstanding efforts of the staff of the Accelerator and the Physics Divisions at Jefferson Lab that made this evaluation of the  $N(1440)1/2^+$ ,  $N(1520)3/2^-$ , and  $\Delta(1620)1/2^-$  electrocouplings and hadronic decay parameters possible. We are grateful to I.G. Aznauryan, V.M. Braun, I.C. Clöet, M.M. Giannini, T-S. H. Lee, M.R. Pennington, C.D. Roberts, E. Santopinto, J. Segovia, and A.P. Szczepaniak for theoretical support and helpful discussions. This work was supported in part by the U.S. Department of Energy and the National Science Foundation, the Skobeltsyn Institute of Nuclear Physics and the Physics Department at Moscow State University, Ohio University, and the University of South Carolina. The Southeastern Universities Research Association (SURA) operates the Thomas Jefferson National Accelerator Facility for the United States Department of Energy under contract DE-AC05-84ER40150.

- 
- [1] I.G. Aznauryan and V.D. Burkert, *Prog. Part. Nucl. Phys.* **67**, 1 (2012).
  - [2] I.G. Aznauryan *et al.*, *Int. J. Mod. Phys.* **E22**, 1330015 (2013).
  - [3] I.C. Clöet and C.D. Roberts, *Prog. Part. Nucl. Phys.* **77**, 1 (2014).
  - [4] I.G. Aznauryan, V.D. Burkert, T-S. H. Lee, and V.I. Mokeev, *J. Phys: Conf. Ser.* **299**, 012008 (2011).
  - [5] V.I. Mokeev and I.G. Aznauryan, *Int. J. Mod. Phys. Conf. Ser.* **26**, 146080 (2014).
  - [6] V.D. Burkert, *Int. J. Mod. Phys. Conf. Ser.* **26**, 146050 (2014).
  - [7] K. Joo *et al.* (*CLAS Collaboration*), *Phys. Rev. Lett.* **88**, 122001 (2002).
  - [8] K. Joo *et al.* (*CLAS Collaboration*), *Phys. Rev. C* **68**, 032201 (2003).
  - [9] K. Joo *et al.* (*CLAS Collaboration*), *Phys. Rev. C* **70**, 042201 (2004).
  - [10] H. Egiyan *et al.* (*CLAS Collaboration*), *Phys. Rev. C* **73**, 025204 (2006).
  - [11] M. Ungaro *et al.* (*CLAS Collaboration*), *Phys. Rev. Lett.* **97**, 112003 (2006).
  - [12] L.C. Smith *et al.* (*CLAS Collaboration*), *Proceedings of the Shape of Hadrons Workshop*, p.222, Athens, 2006.
  - [13] K. Park *et al.* (*CLAS Collaboration*), *Phys. Rev. C* **77**, 015208 (2008).
  - [14] A. Biselli *et al.* (*CLAS Collaboration*), *Phys. Rev. C* **78**, 045204 (2008).
  - [15] K. Park *et al.* (*CLAS Collaboration*), *Phys. Rev. C* **91**, 045203 (2015).
  - [16] H. Denizli *et al.* (*CLAS Collaboration*), *Phys. Rev. C* **76**, 015204 (2007).
  - [17] D.S. Carman *et al.* (*CLAS Collaboration*), *Phys. Rev. C* **87**, 025204 (2013).
  - [18] R. Nasseripour, *et al.* (*CLAS Collaboration*), *Phys. Rev. C* **77**, 065208 (2008).
  - [19] P. Ambrozewicz, *et al.* (*CLAS Collaboration*), *Phys. Rev. C* **75**, 045203 (2007).
  - [20] M. Gabrielyan *et al.* (*CLAS Collaboration*), *Phys. Rev. C* **90**, 035202 (2014).
  - [21] D.S. Carman *et al.* (*CLAS Collaboration*), *Phys. Rev. C* **79**, 065205 (2009).
  - [22] D.S. Carman *et al.* (*CLAS Collaboration*), *Phys. Rev. Lett.* **90**, 131804 (2003).
  - [23] G.V. Fedotov *et al.* (*CLAS Collaboration*), *Phys. Rev. C* **79**, 015204 (2009).
  - [24] M. Ripani *et al.* (*CLAS Collaboration*), *Phys. Rev. Lett.* **91**, 022002 (2003).
  - [25] I.G. Aznauryan *et al.* (*CLAS Collaboration*), *Phys. Rev. C* **80**, 055203 (2009).
  - [26] V.I. Mokeev *et al.*, *Phys. Rev. C* **80**, 045212 (2009).
  - [27] V.I. Mokeev *et al.* (*CLAS Collaboration*), *Phys. Rev. C* **86**, 055203 (2012).
  - [28] V.M. Braun *et al.*, *Phys. Rev. Lett.* **103**, 0722001 (2009).

- [29] I.V. Anikin, V.M. Braun, and N. Offen, Phys. Rev. D **92**, 014018 (2015).
- [30] V. M. Braun *et al.*, Phys. Rev. D **89**, 0722001 (2014).
- [31] J. Segovia *et al.*, Few Body Syst. **55**, 1185 (2014).
- [32] D. Binosi, L. Chang, J. Papavassiliou, and C.D. Roberts, Phys. Lett. B **742**, 183 (2015).
- [33] J. Segovia *et al.*, arXiv:1504.04386 [nucl-th].
- [34] G. Eichmann and D. Nicmorus, Phys. Rev. D **85**, 093004 (2012).
- [35] I.C. Clöet, C.D. Roberts and A.W. Thomas, Phys. Rev. Lett. **111**, 101803 (2013).
- [36] M.M. Giannini and E. Santopinto, Chin. J. Phys **53**, 020301 (2015).
- [37] M. Ronninger and B. Ch. Metsch, Eur. Phys J. A **49**, 8 (2012).
- [38] G. Ramalho and M. T. Pena, Phys. Rev. D **89**, 094016 (2014).
- [39] G. Ramalho and K. Tsushima, Phys. Rev. D **81**, 074020 (2010).
- [40] T. Bauer, S. Scherer and L. Tiator, Phys. Rev. C **90**, 015201 (2014).
- [41] N. Suzuki, T. Sato, and T.-S. H. Lee, Phys. Rev. C **82**, 045206 (2010).
- [42] B. Julia-Diaz *et al.*, Phys. Rev. C **80**, 025207 (2009).
- [43] B. Julia-Diaz *et al.*, Phys. Rev. C **77**, 045205 (2008).
- [44] I.G. Aznauryan and V.D. Burkert, arXiv:1412.1296 [nucl-th].
- [45] I.G. Aznauryan and V.D. Burkert, Phys. Rev. C **85**, 055202 (2012).
- [46] I.T. Obukhovskiy *et al.*, Phys. Rev. D **89**, 0142032 (2014).
- [47] B. Golli and S. Sirca, Eur. Phys. J. A **49**, 111 (2013).
- [48] B. Golli and S. Sirca, Eur. Phys. J. A **42**, 185 (2009).
- [49] E. Santopinto and M.M. Giannini, Phys. Rev. C **86**, 065202 (2012).
- [50] E. Byckling and K. Kajantie, Particle Kinematics, John Wiley & Sons 1972.
- [51] M. Ripani *et al.*, Nucl. Phys. A **672**, 220 (2000).
- [52] I.G. Aznauryan *et al.*, Phys. Rev. C **72**, 045201 (2005).
- [53] I.J.R. Aitchison, Nucl. Phys. A **189**, 417 (1972).
- [54] I.J.R. Aitchison and J.J. Brehm, Phys. Rev. D **17**, 3072 (1978).
- [55] M. Guidal, J.-M. Laget, and M. Vanderhaeghen, Nucl. Phys. A **627**, 645 (1997).
- [56] M. Guidal, J.-M. Laget, and M. Vanderhaeghen, Phys. Lett. B **400**, 6 (1997).
- [57] V.D. Burkert *et al.*, Phys. Atom. Nucl. **70**, 427 (2007).
- [58] T-S. H. Lee, AIP Conf. Proc. **1560**, 413 (2013).
- [59] H. Kamano *et al.*, Phys. Rev. C **80**, 065203 (2009).
- [60] I.G. Aznauryan *et al.*, Phys. Rev. C **71**, 015201 (2005).
- [61] V.I. Mokeev *et al.*, in “Proc. of the Workshop on the Physics of Excited Nucleon. NSTAR2005”, ed. by S. Capstick, V. Crede, P. Eugenio, World Scientific Publishing Co., p. 47.
- [62] V.D. Burkert *et al.*, Phys. Rev. C **67**, 035204 (2003).
- [63] M. Shi *et al.*, Phys. Rev. D **91**, 034007 (2015).
- [64] H. Kamano *et al.*, PoS Hadron2013 112 (2013).
- [65] V.I. Mokeev, I.G. Aznauryan, and V.D. Burkert, Proc. of 21st Int. Conf. on Few Body Problems in Physics, in preparation.
- [66] I.G. Aznauryan, V.D. Burkert, and V.I. Mokeev, AIP Conf. Proc. **1432**, 68 (2012).
- [67] L. Tiator *et al.*, Eur. Phys. J. ST **198**, 141 (2011).
- [68] K. A. Olive *et al.*, Chin. Phys., Phys. C **38**, 090001 (2014).
- [69] D.M. Manley and E.M. Salesky, Phys. Rev. D **45**, 4002 (1992).
- [70] J. Segovia, C.D. Roberts, and S.M. Schmidt, arXiv:1506.05112 [nucl-th].
- [71] I.G. Aznauryan and V.D. Burkert, Phys. Rev. C **92**, 015203 (2015).
- [72] T.M. Aliev and M. Savci, Phys. Rev. D **90**, 096012 (2014).
- [73] E. Santopinto and J. Ferretti, EPJ Web Conf. **96**, 01026 (2015).
- [74] R.W. Gothe *et al.*, Nucleon Resonance Studies with the CLAS12, JLab Experiment E12-09-003.
- [75] D.S. Carman *et al.*, Exclusive  $N^* \rightarrow KY$  Studies with CLAS12, JLab Experiment E12-06-108A.
- [76] G.V. Fedotov and R. W. Gothe, AIP Conf. Proc. **1432**, 203 (2012).
- [77] S.J. Brodsky *et al.*, QCD and Hadron Physics. Summary of the DNP Town Meeting Temple University, 13-15 September 2014, arXiv:1502.05728 [hep-ph].